

# Protracted localization of metamorphism and deformation in a heterogeneous lower-crustal shear zone

Sascha Zertani<sup>a,\*</sup>, Luca Menegon<sup>a</sup>, Giorgio Pennacchioni<sup>b</sup>, Iris Buisman<sup>c</sup>, Fernando Corfu<sup>d</sup>, Bjørn Jamtveit<sup>a</sup>

<sup>a</sup> Njord Centre, Department of Geosciences, University of Oslo, Oslo, Norway

<sup>b</sup> Department of Geosciences, Università di Padova, Padova, Italy

<sup>c</sup> Department of Earth Sciences, University of Cambridge, Cambridge, United Kingdom

<sup>d</sup> Centre of Earth Evolution and Dynamics (CEED), Department of Geosciences, University of Oslo, Oslo, Norway

## ARTICLE INFO

### Keywords:

Shear zones  
Brittle/ductile deformation  
Metamorphism  
Continental crust  
Fluid-rock interaction  
Microstructures

## ABSTRACT

Deformation of the continental crust is influenced by the pre-existing structural framework, fluid availability, strain rate, and pressure-temperature conditions. We investigate the evolution of a large (hundreds-of-meters wide) heterogeneous shear zone and associated brittle and ductile deformation structures (Lofoten, Norway) using structural analysis, mineral-chemical and microstructural observations, and U-Pb dating. The shear zone developed through a sequence of metamorphic stages: (1) migmatization and granulite-facies metamorphism, (2) eclogite-facies metamorphism, and (3) amphibolite-facies metamorphism. Stage (1) was related to magmatic activity at lower-crustal conditions prior to 1.7 Ga. Stage (2) likely occurred during the early phases of the collision between Baltica and Laurentia (Caledonian collision). Stage (3) was related to shortening during the main phase of the Caledonian collision (~430–400 Ma) and was accompanied by hydration of the shear zone. We demonstrate how mechanical heterogeneities influence the deformation style from the centimeter to meter scale. Zones with a pre-existing fabric deformed by ductile shearing and folding, whereas homogeneous, dry rocks fractured. Fractures provided precursors for small-scale shear zones. These contrasting deformation styles occurred repeatedly. Consequently, pre-existing structures define the deformation style and serve as conduits for the channelization of fluids over extended periods of time.

## 1. Introduction

The deformation of the continental crust plays a critical role in the evolution of orogens (e.g., Andersen et al., 1991; Jackson et al., 2004; Jamtveit et al., 2019). Classical models of crustal strength predict a transition from brittle failure to ductile flow at depths of ~10–15 km, and that a weak, ductile lower crust is sandwiched between a strong upper crust and a strong upper mantle. If the lower crust is dry, however, it is predicted to be very strong (McKenzie and Jackson, 2002; Bürgmann and Dresen, 2008). This is supported by several examples of exhumed lower crust that demonstrate that these dry rocks require brittle failure and fluid infiltration in order to weaken and flow (e.g., Austrheim, 1987; Jamtveit et al., 1990; Jolivet et al., 2005; Menegon et al., 2017; Giuntoli et al., 2018b; Wex et al., 2018; Zertani et al., 2019; Kaatz et al., 2021). Consequently, the mechanisms by which the lower crust deforms are dependent on the availability of fluids, temperature,

and the strain rate (Campbell and Menegon, 2019; Papa et al., 2020).

Models of crustal strength commonly assume that the lower crust is isotropic and homogeneous, while field observations from exhumed lower-crustal sections indicate that it is structurally and compositionally heterogeneous. In this context, deformation in otherwise massive rocks localizes on/along pre-existing structures, e.g., fractures, foliation planes, dykes, or any other planar structural heterogeneity (Pennacchioni, 2005; Pennacchioni and Mancktelow, 2007; Menegon et al., 2017; Corvò et al., 2022). For instance, Pennacchioni and Mancktelow (2007) describe amphibolite-facies shear zones that nucleate on fractures and dykes within an otherwise homogenous granodiorite in the Tauern window (eastern Alps). On a larger scale, Ceccato et al. (2020) have demonstrated that the geometry of Caledonian folding in the Kalak nappe (Norway) is controlled by the orientation of pre-Caledonian fabrics.

Likewise, metamorphic reactions can be localized into ductile shear

\* Corresponding author. Postboks 1048 Blindern, 0316, Oslo, Norway.

E-mail address: [sascha.zertani@mn.uio.no](mailto:sascha.zertani@mn.uio.no) (S. Zertani).

<https://doi.org/10.1016/j.jsg.2023.104960>

Received 20 April 2023; Received in revised form 15 September 2023; Accepted 21 September 2023

Available online 28 September 2023

0191-8141/© 2023 The Authors. Published by Elsevier Ltd. This is an open access article under the CC BY license (<http://creativecommons.org/licenses/by/4.0/>).

zones leaving low-strain zones largely unaffected by metamorphic re-equilibration (Austrheim, 1987; Molli et al., 2006; Zertani et al., 2019). Specifically, the availability of fluids plays an important role in this regard, as the presence of fluids increases reaction kinetics and thus the re-equilibration to changing P-T conditions, while deformation along shear zones can lead to channelized fluid flow (Oliver, 1996; Fousseis et al., 2009; Menegon et al., 2015; Zertani et al., 2022).

One example of a lower-crustal section composed of dry mafic magmatic and granulitic rocks is exposed in the Lofoten archipelago (northern Norway). Here, pseudotachylytes - solidified frictional melts that are interpreted as evidence of paleo-seismicity - are described to have formed cyclically with ductile shear zones (Menegon et al., 2017; Campbell et al., 2020). These shear zones exploited pseudotachylytes as precursors. Lofoten is well known as a natural laboratory to study earthquake processes and the interplay of seismic failure and aseismic flow (e.g., Steltenpohl et al., 2006; Jamtveit et al., 2019; Incel et al., 2020; Dunkel et al., 2021; Menegon et al., 2021; Campbell and Menegon, 2022; Michalchuk et al., 2023). However, the tectonic setting in which this seismicity occurred remains debated, as the position of the Lofoten block during the Caledonian collision is unclear. A debated issue is the age of eclogite-facies metamorphism, locally preserved in the geological record. Steltenpohl et al. (2011) reported an age of  $478 \pm 41$  Ma, based on a long extrapolation of discordant zircon U-Pb data. Jaranowski et al. (2023) obtained an age of  $427 \pm 6$  Ma, which is also based on zircon U-Pb data. Froitzheim et al. (2016) obtained a Lu-Hf age of 399

$\pm 10$  Ma for garnet (and omphacite). This uncertainty in the timing complicates determining a model for the eclogite-facies event, and consequently for the tectonic context in which the seismicity occurred.

Here we present a detailed structural and petrological analysis of one of the eclogite localities (e.g. Froitzheim et al., 2016) in Lofoten (Ramberg, Flakstadøya; Fig. 1). Our observations indicate that the exposed lower-crustal shear zone has been repeatedly exploited for deformation and metamorphism over an extended period of time. The microstructures in this shear zone preserve evidence of granulite-facies, eclogite-facies, and amphibolite-facies re-equilibration. Using field-based and microstructural observations combined with mineral-chemical and textural analyses, as well as thermodynamic calculations, we untangle this complex history of metamorphism and deformation. We demonstrate that structural heterogeneities influence the deformation style over very long timescales and that the same structures serve as long-lived fluid conduits. Furthermore, the results shed new light on the tectonic evolution of the Lofoten block.

## 2. Geological setting

The Lofoten-Vesterålen archipelago (northern Norway) preserves a block of lower continental crust that largely escaped Caledonian re-equilibration (Griffin et al., 1978; Corfu, 2004). The dominant lithologies are AMCG (anorthosite, monzonite, charnockite, granite) suite

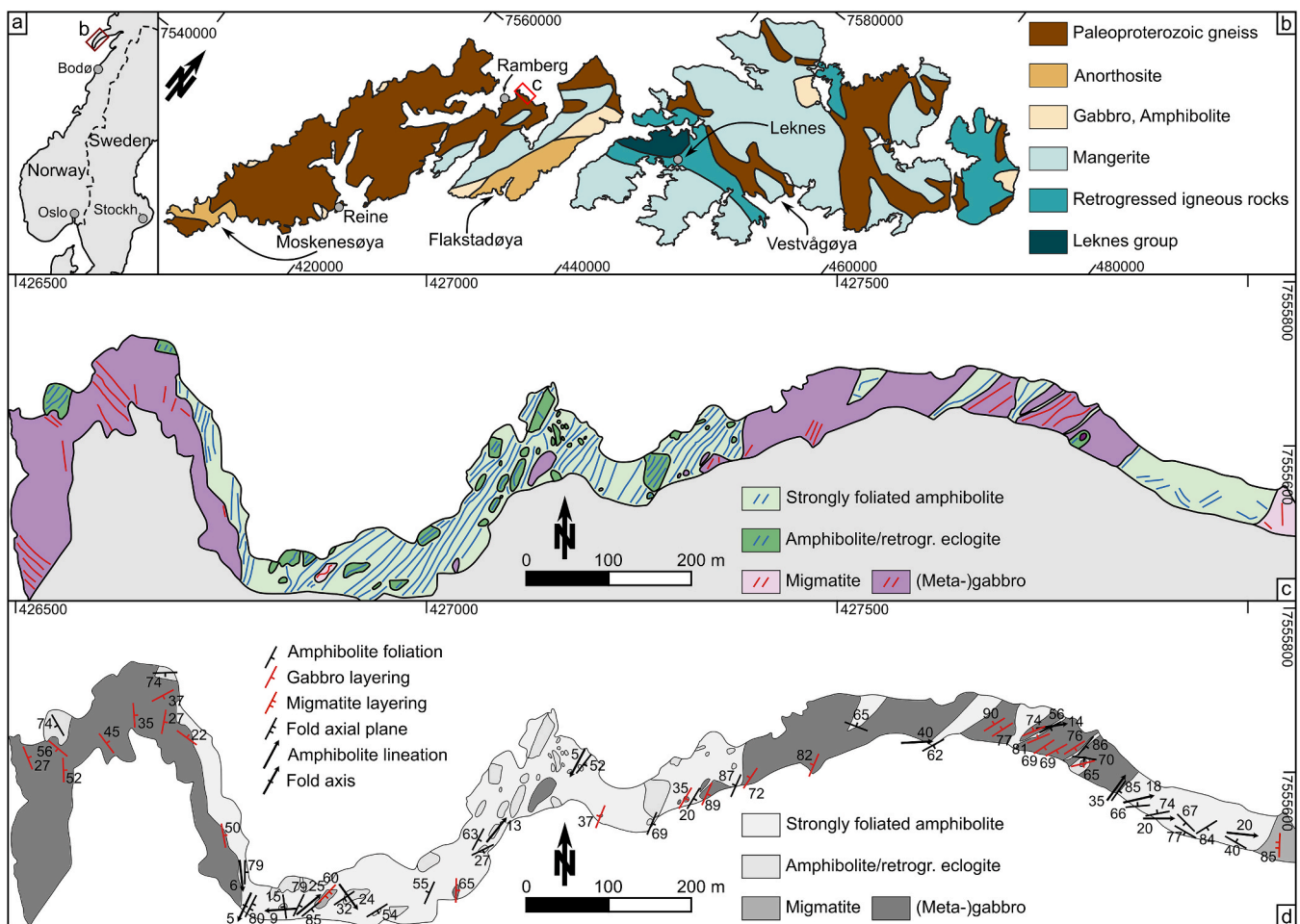


**Fig. 1.** Geological maps of the studied area. a) Map of Norway and Sweden showing the location of Lofoten in northern Norway (red box); Stockh. – Stockholm. b) Geological map of the Lofoten islands Moskenesøya, Flakstadøya, and Vestvågøya (modified from Griffin et al., 1978), showing the distribution of the dominantly magmatic suite lithologies. The red box shows the location of the Ramberg locality. Water is shown in white and areas without rock exposure in grey. Foliation trends are shown in blue and red lines (see figure legend). c) Structural map of the Ramberg locality. Water is shown in white and areas without rock exposure in grey. Foliation trends are shown in blue and red lines (see figure legend). d) The same map as in c) showing measured fabric orientations. Coordinates refer to UTM Zone 33 north.

rocks that intruded into Archean to Paleoproterozoic gneisses at granulite-facies conditions around  $\sim 1.9$ – $1.7$  Ga (Markl et al., 1998; Corfu, 2004; Fig. 1).

The subsequent tectonic evolution of the Lofoten block is unclear as it dominantly preserves magmatic and granulite-facies mineral assemblages and fabrics with a volumetrically minor Caledonian overprint, even though the crustal block presumably occupied an internal position during collision (Roberts and Gee, 1985). This minor overprint is dominantly preserved by abundant pseudotachylytes and amphibolite-facies shear zones that typically exploited the pseudotachylytes as precursor structures (Menegon et al., 2017; Campbell et al., 2020; Dunkel et al., 2021). The other expression of the Caledonian event is the minor occurrence of eclogites (Steltenpohl et al., 2011; Froitzheim et al., 2016).

Eclogites in Lofoten have only been reported from a few localities: Ramberg, Myrland, Storvatnet, Vikten, Nusfjord, and Napp (Markl and Bucher, 1997; Kullerud et al., 2001; Steltenpohl et al., 2003, 2006; Froitzheim et al., 2016). These eclogites were typically strongly retrogressed during later amphibolite-facies metamorphism (Steltenpohl et al., 2011). Estimates of eclogitization conditions are variable from 2.5 to 2.8 GPa and  $\sim 650$  °C, based on conventional thermobarometry and thermodynamic modeling (Froitzheim et al., 2016), to 1.1–1.5 GPa and 680–780 °C, based on multi-equilibrium calculations (Markl and Bucher, 1997).

### 3. Methods

Sampling and structural analysis was conducted in Lofoten just east of the town Ramberg. All structural measurements were corrected for a declination of  $+6^\circ$ . Orientation plots were made using the MATLAB toolbox of Allmendinger et al. (2011).

Backscattered electron (BSE) images were collected on a Hitachi SU5000 FE scanning electron microscope at the Department of Geosciences, University of Oslo, using an acceleration voltage of 15 kV and a working distance of 11–12 mm. The same instrument was used for phase identification and qualitative compositional mapping by energy dispersive spectrometer (EDS) analysis and for electron backscatter diffraction (EBSD) analysis using the Bruker e-Flash detector. Operating conditions were 20 kV acceleration voltage, a working distance of 22 mm,  $70^\circ$  sample tilt, a step size of 0.3  $\mu\text{m}$ , and 40 ms exposure time. Indexing of EBSD patterns was performed using the Esprit software (v. 2.3; Bruker) and EBSD data was post-processed and visualized using the MTEX toolbox v. 5.5.2 (Bachmann et al., 2010). Additional BSE images were acquired with a Hitachi TM4000 Plus Tabletop scanning electron microscope at the Department of Geosciences, University of Oslo, using an acceleration voltage of 15 kV and a working distance of 11–12 mm.

Qualitative compositional maps of garnet (Grt) were acquired with a JEOL JXA-iHP200F Field Emission electron probe micro analyzer at the Department of Earth Sciences, University of Cambridge. The instrument is equipped with five wavelength dispersive spectrometers (WDS) that were used to measure P, Ti, Na, Ca, and Mg. Simultaneously, Fe, Mn, Si, Al, and Cr were analyzed using the EDS detector. Compositional maps were acquired using a step size of 1 or 2  $\mu\text{m}$  (depending on the size of the target area), 20 kV acceleration voltage, 300 nA beam current, and 200 ms dwell time. Color maps are from Crameri (2018). Quantitative point analyses were acquired on a Cameca SX100 electron micro probe at the Department of Geosciences, University of Oslo, using 1  $\mu\text{m}$  beam diameter, 15 kV acceleration voltage, and beam currents of 20 nA for Grt, amphibole (Amp), and clinopyroxene (Cpx), and 10 nA for plagioclase (Pl; all mineral abbreviations after Whitney and Evans, 2010).

Thermodynamic calculations were performed by Gibbs energy minimization using Thermolab (v. 22.03.23; Vrijmoed and Podladchikov, 2022) using the thermodynamic data for Cpx (Green et al., 2007), ternary feldspar (Holland and Powell, 2003), and quartz (Qz; Holland and Powell, 1998). The following compositions were used (in mol): (1) Si = 5, Al = 0.8, Fe = 0.4, Ca = 1.0, Mg = 0.8, Na = 1.0, O = 14.0; (2) Si

= 5, Al = 0.4, Fe = 0.4, Ca = 1.4, Mg = 1.2, Na = 0.6, O = 14.0, which correspond to two formula units of omphacite (Omp) + Qz for a jadeite (Jd)<sub>40</sub> (1) and Jd<sub>20</sub> (2) composition. Qz was added because it is required to balance the reaction (Anderson and Moecher, 2007).

Dating was carried out by the U-Pb isotope dilution thermal ionisation mass spectrometry method at the Department of Geosciences, University of Oslo. The rock samples were processed using a jaw crusher and pulverizer, and zircon was concentrated using Wilfley table, and magnetic and heavy liquid separation. The selected grains were pretreated by chemical abrasion (Mattinson, 2005). The U-Pb analytical procedure followed the general procedure of Krogh (1973) with modifications and quality procedures described in Corfu (2004). Decay constants are from Jaffey et al. (1971). Plotting and calculations were done with Isoplot (Ludwig, 2009).

## 4. Field observations

### 4.1. Lithologies and field relationships

The studied area comprises gabbroic rocks and amphibolites exposed along a  $\sim 1.5$  km shore section east of the village Ramberg on Flakstadøya (Fig. 1b). The western and eastern parts of the section expose dominantly undeformed gabbros showing a weak magmatic layering. The mean orientation of this layering is 078/36 (dip azimuth/dip) in the west and 293/82 in the east. Locally, the rocks preserve a migmatitic layering (Fig. 2a).

The central part of the area consists of a 600–700 m thick shear zone (Fig. 1c) of dominantly, strongly foliated amphibolites. The penetrative foliation (Fig. 2b) anastomoses around meters to tens-of-meters sized low-strain domains, which is reflected in a scattering in orientation (Fig. 3a) around the dominant orientation of  $\sim 115/75$ . Likewise, the mineral lineations are scattered, plunging shallowly to the SSW,  $\sim$ E, and NNE with a distribution maximum oriented parallel to a SSW-NNE trend (Fig. 3b). Shear sense indicators are rare and features are commonly symmetric. The few observed kinematic indicators dominantly record sinistral movement along the steeply-dipping foliation (Fig. 2b). In one outcrop, the foliation is crenulated (Fig. 2c), with steeply SE-dipping fold axial planes and sub-horizontal fold axes trending SSW-NNE (Fig. 3c). The shear zone foliation is cut by straight to weakly folded pegmatite dykes (Fig. 2d). A strongly folded mafic dyke was found (Fig. 2e; fold axis 351/38).

Low-strain domains are either composed of gabbros or weakly to non-foliated amphibolites, some of which contain microscopic relicts of eclogite-facies minerals (see Section 5.4). In the latter case, the rocks are coarser grained than those forming the main foliation, and their weak foliation is (sub-)parallel to the foliation of the shear zone. The amphibolite foliation at contacts to migmatite or layered gabbro is parallel to the migmatitic or the gabbro layering (Fig. 2e and f).

The gabbros, both outside the main shear zone and within low-strain domains, frequently contain veins and shear zones with a thickness of  $\sim 1$ – $10$  cm (small-scale shear zones in the following; Pennacchioni and Mancktelow, 2018), that are discordant to the magmatic layering of the gabbro. Veins are characterized by a surrounding alteration halo, which is either white (bleached) or greenish (Fig. 4a and b). The small scale-shear zones may be localized on the central vein (Fig. 5b), or form paired shear zones flanking the alteration halos surrounding the central vein (Fig. 4c and d). In rare cases, small-scale shear zones intersect, in which case they are mutually offsetting, with the formation of thinned zones at the intersection (Pennacchioni and Mancktelow, 2007; Fig. 5). The foliation of the eastern occurrence of amphibolite (Figs. 1 and 3) is more variable, and because of the more limited exposures the structural architecture is somewhat unclear (see Fig. 3e).

### 4.2. Structural analysis

The schematic cross section in Fig. 3e illustrates the structural

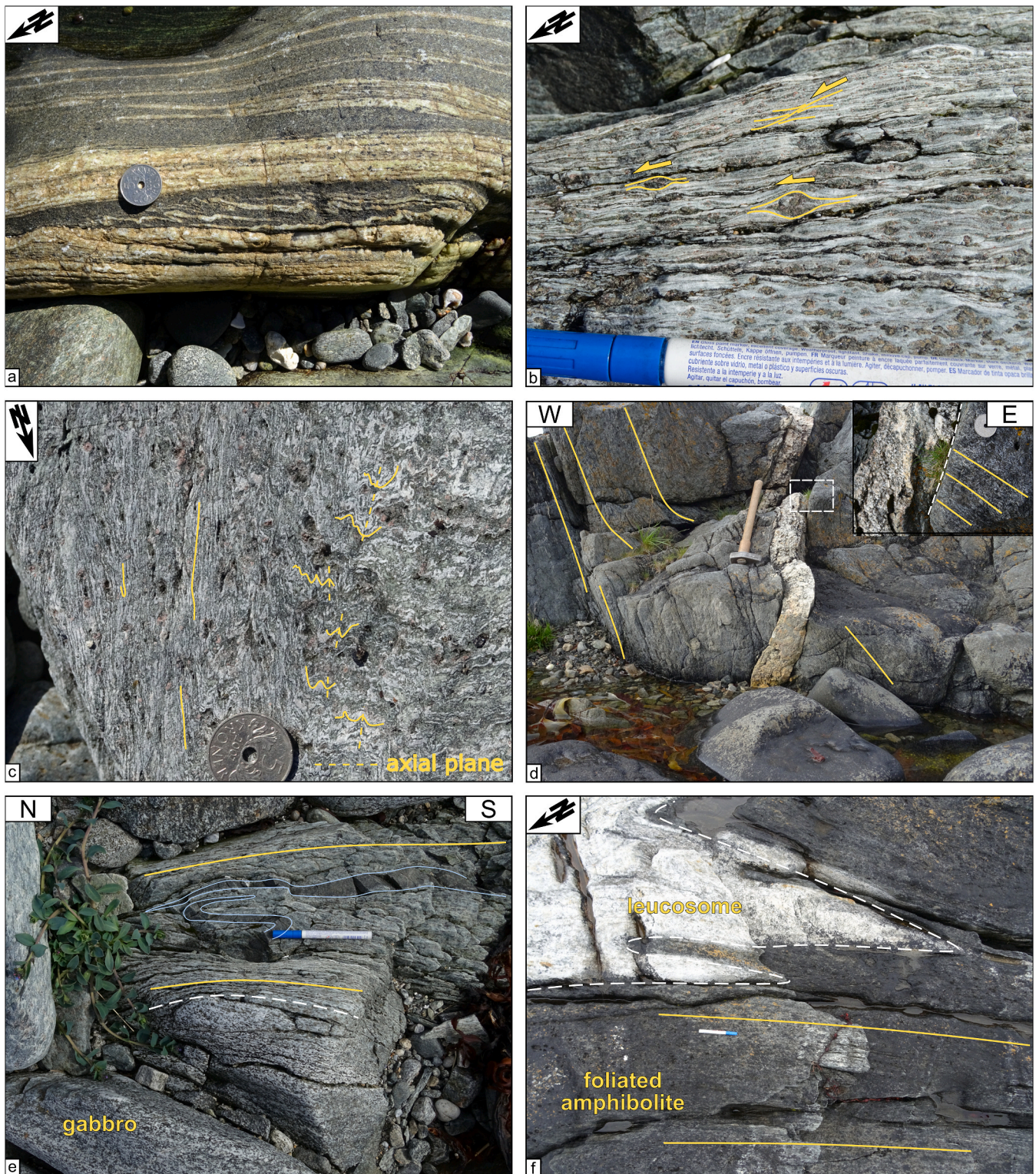


**Fig. 2.** Photographs of key occurrences exposed at the Ramberg locality. a) Migmatite. b) Foliated amphibolite that forms the main deformation fabric. Local shear bands and  $\sigma$ -clasts indicate sinistral (top view) kinematics. c) Folding of an amphibolite fabric (right) and a foliation parallel to the fold axial plane (left). Top view, fold axes plunge shallowly to the ~south in this image. Dashed lines show the trace of the fold axial plane. d) Weakly folded pegmatite dyke that cross-cuts the amphibolite foliation (see inset top right, location given by white box). e) Transition of the foliated amphibolite (yellow) to a preserved gabbro block. The transition is characterized by a sharp contact (white dashed line) to the undeformed gabbro. Layers of more competent mafic material (highlighted in blue) are folded with the fold axial plane parallel to the foliation. f) Transition from the migmatite to the foliated amphibolite. The foliation (yellow) is parallel to the dominant layering of the migmatite.

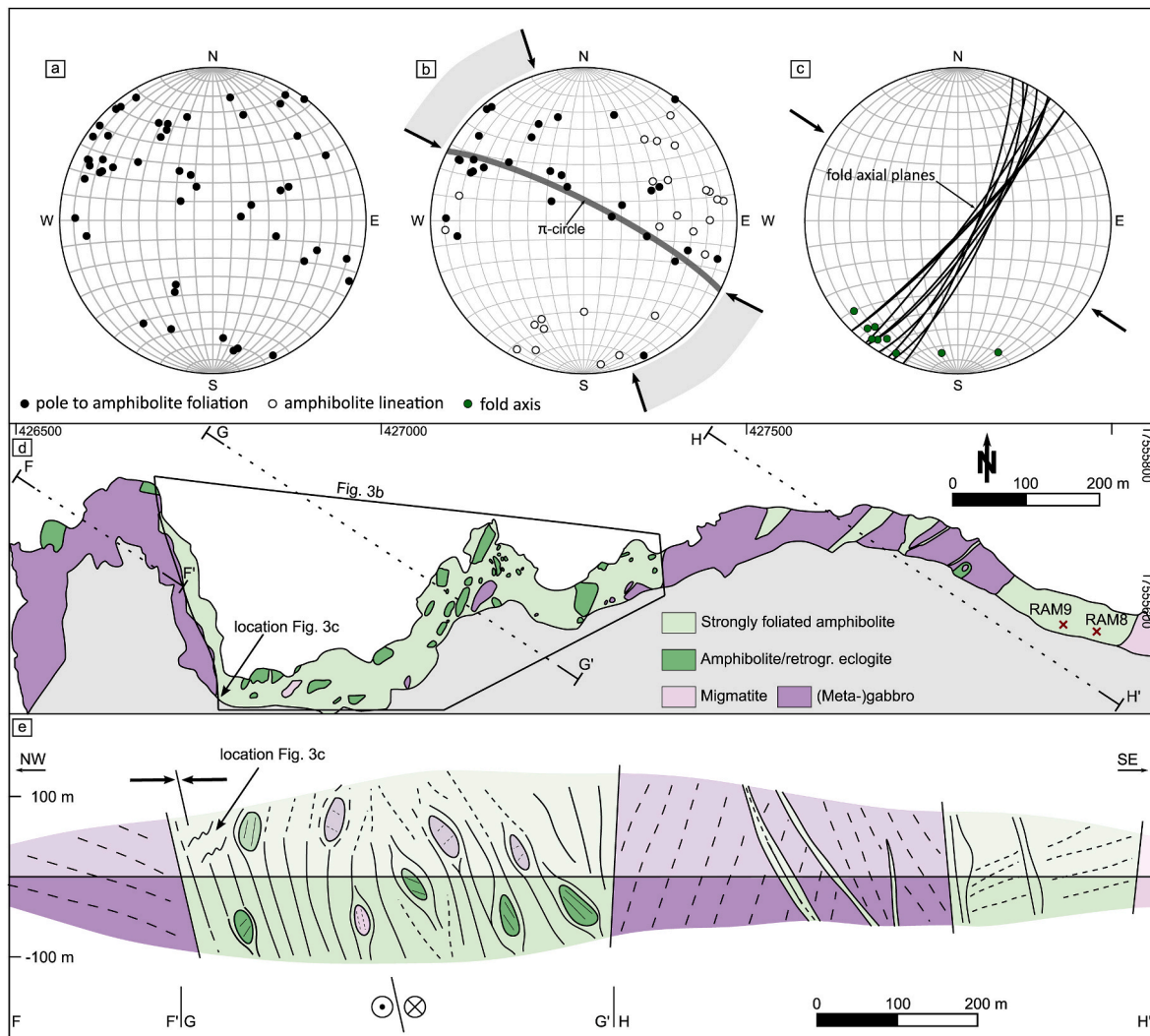


**Fig. 3.** Structural relationships of the Ramberg locality. a)–c) are equal-area lower-hemisphere projections of orientations measured along the shore line. a) Poles to the amphibolite foliation along the entire section. b) Poles to the amphibolite foliation (black) measured within the main shear zone branch (polygon in d), and corresponding lineations (open symbols). The  $\pi$ -circle is calculated from the data in c (see main text for details). c) Fold axial planes of the crenulation folds and corresponding fold axes (green). The mean value of these fold axes is used to calculate the  $\pi$ -circle in b (see main text). Arrows show inferred shortening directions. d) Geological map from Fig. 1c showing the locations of b and c as well as the schematic cross-section shown in e. RAM8 and RAM9 mark the location of dated pegmatite dykes. e) Schematic cross-section showing foliation trends.

relationships in the studied area. The orientation of the magmatic layering of gabbros is relatively constant in the western part of the section (Fig. 1c), dipping moderately towards NE and E. The gabbro layering in the eastern part is dominantly steep, dipping to the SE and NW (Fig. 1d). In this area, the gabbro is volumetrically dominant and is cut by meter to tens-of-meters wide amphibolite shear zones (Figs. 1d and 3e). In the central part of the section, the gabbro occurs only as meter-sized lenses and the section is dominated by the amphibolite-facies mylonitic fabric.

The main shear zone fabric is dominantly steep but variable (Fig. 3a–b, e). Small-scale folding may indicate larger-scale folding but determination of the orientation of a corresponding fold axis is complicated due to the spread of orientations, rendering a straightforward determination of a  $\pi$ -circle difficult. We thus use the fold axes measured from the crenulation and reconstruct the orientation of the corresponding  $\pi$ -circle. Plotting of this  $\pi$ -circle together with the poles to the main foliation shows that a significant number of data points plots along the  $\pi$ -circle (Fig. 3b).

Two sets of mutually offsetting, intersecting small-scale shear zones with thinned intersection zones were found in gabbro blocks (Fig. 5).

Both of the blocks hosting the shear zones have a magmatic layering with a different orientation than in the western or eastern part of the studied area, one of which may represent the original orientation. Fig. 5 shows lower hemisphere equal-area projections of the rotation, assuming the magmatic layering in the east represents the original orientation. As the direction of rotation is unknown both possibilities are shown in the projections (Fig. 5). The shortening direction is assumed to be the bisector angle perpendicular to the thinned intersection zone (yellow arrows in Fig. 5). This shortening direction is rotated together with the shear zones (black arrows in Fig. 5). Angles between the magmatic layering of the block and the magmatic layering in the western part of the study area are  $96^\circ$  (counter-clockwise) and  $84^\circ$  (clockwise) in Fig. 5a, and  $134^\circ$  (counter-clockwise) and  $46^\circ$  (clockwise) in Fig. 5b. Rotating the shear zones using this procedure results in shortening directions of NW ( $302^\circ$  and  $301^\circ$ ) - SE ( $122^\circ$  and  $121^\circ$ ; Fig. 5a) and NW ( $323^\circ$ ) - SE ( $143^\circ$ ) and NE ( $45^\circ$ ) - SW ( $225^\circ$ ; Fig. 5b). An analysis, that assumes the orientation of the magmatic layering in the western part of the study area as the original orientation, is presented in the supplementary material (Fig. S1).



Fig. 4. Examples of veins with surrounding alteration haloes and associated small-scale shear zones in the studied area. a) Central vein surrounded by a bleached halo; b) Central vein surrounded by a greenish halo; c) Heterogeneous small-scale shear zone exploiting a central fracture still visible in the shear zone core; d) Paired shear zones exploiting the border of a greenish alteration halo surrounding a central vein.

## 5. Microstructural description

### 5.1. Gabbro (host rock)

The gabbroic host rock (gabbro-norite) is dominantly composed of coarse-grained (~3–5 mm) Pl, interspersed aggregates of orthopyroxene (Opx) and Cpx, and minor olivine, and Fe-(Ti)-oxides.

### 5.2. Foliated amphibolite (main shear zone)

The foliated amphibolites are composed of a fine to medium-grained (<10–200  $\mu\text{m}$ ) matrix of Amp and Pl, with variable amounts of Qz, including distributed Grt porphyroclasts. Biotite (Bt), kyanite (Ky), rutile, titanite, pyrite, and apatite occur in accessory amounts. The foliation is defined by the moderate to strong shape preferred orientation (SPO) of Amp and by a compositional layering related to grain size variations of the Amp-Pl aggregates (Fig. 6a). The foliation wraps around the Grt porphyroclasts and coarser-grained domains of Amp and Pl. Grt is inclusion-rich including Omp. The inclusion assemblages and microstructures of Grt are described in more detail in Sections 6 and 7.

The Amp grain size varies between <50 and 200  $\mu\text{m}$  and variations may occur in alternating bands or patches. Typically, coarser Amp is found adjacent to Grt. Amp compositions are pargasite, edenite, to magnesiohornblende. Transitions are gradual and EMPA analyses do not indicate a systematic relationship between changes of chemical composition and the microstructural position of Amp (Fig. 7a and b). Pl (An<sub>45-18</sub>; Fig. 7c), similarly to Amp, shows coarser aggregates commonly arranged in Grt tails. Most samples contain no, or only very little,

interstitial Qz within the matrix. Some rare examples include polycrystalline Qz ribbons (Fig. 6a).

In crenulated samples, folding affects alternating Amp-rich and Pl-rich bands (Fig. 6c). There is neither evidence of the development of a new axial planar foliation nor of breakdown of the Amp-Pl dominated assemblage during folding.

Within the matrix, symplectites of Cpx and Pl (Cpx-Pl symplectites) occur, but only in samples where Grt has Omp inclusions. Cpx-Pl symplectites locally have sigmoidal shapes and their core typically preserves the pristine vermicular microstructure (Fig. 6b). Pl in the symplectites is Na-richer than the matrix Pl (Fig. 8). The Cpx-Pl symplectites include some minor Amp and are completely rimmed by Amp.

### 5.3. Small-scale shear zones

Small-scale shear zones (sensu Pennacchioni and Mancktelow, 2018), a few millimeters to a few centimeters thick, are dominantly composed of a Pl and Amp aggregate. Some shear zones contain corona-type microstructures, typically with Opx core, mantled by Cpx and/or Amp, and an outer Grt rim. These coronas are flattened parallel to the shear plane. In the larger grains, Cpx is replaced by Amp along cleavage planes. Grt may occur distributed throughout the matrix, as clusters, or lining the boundary of larger preserved host rock porphyroclasts. In addition to Pl and Amp, the matrix includes Ky and spinel. Away from the coronas, Pl can be zoned with increasing An content from core to rim (inverse zoning, Fig. 6d). Here, Pl can have a significant SPO defining the foliation in samples that contain less Amp. The mineral chemistry of Amp and Pl is the same as in the foliated amphibolite

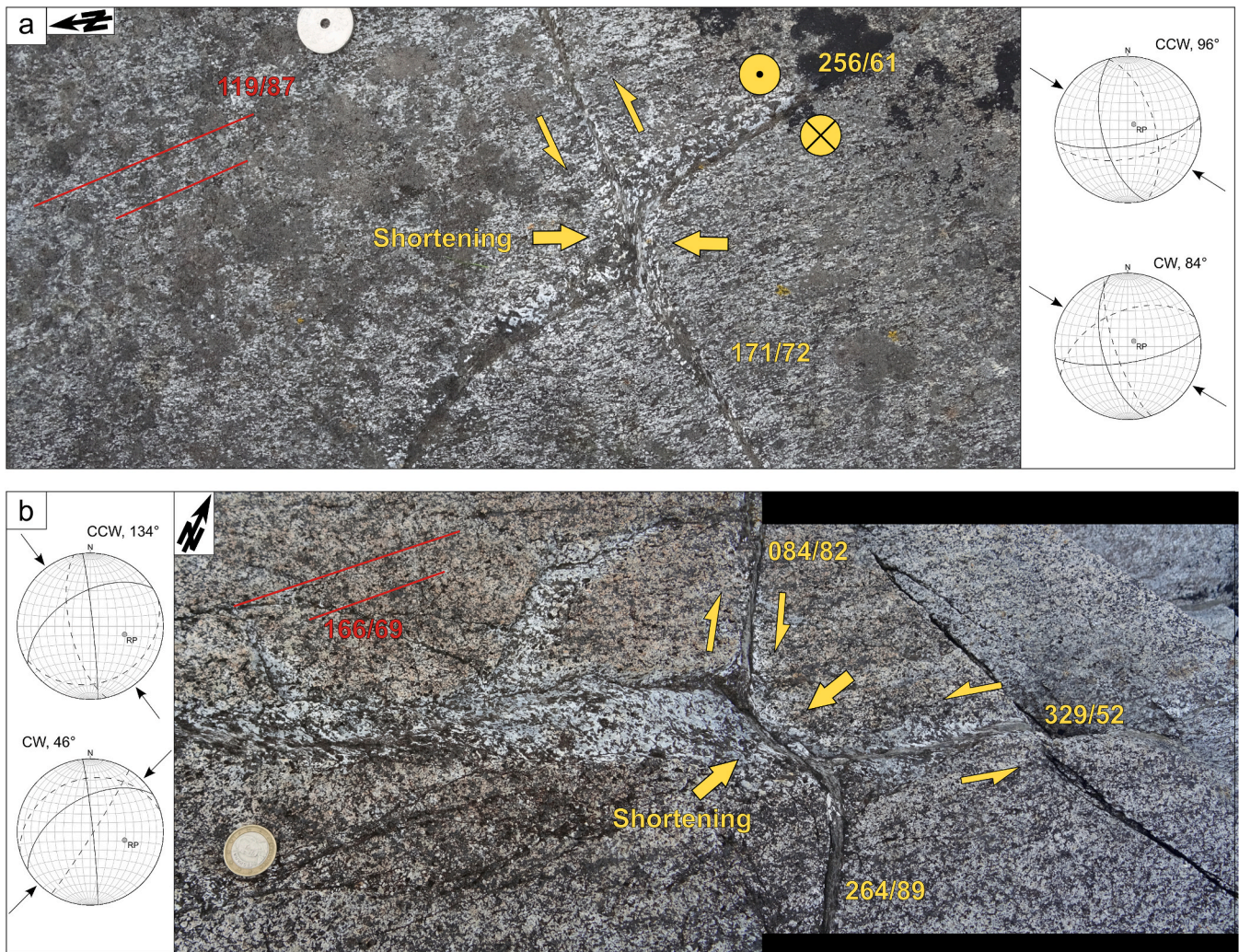


**Fig. 5.** Examples of intersecting small-scale shear zones. Shear zone orientations are given as dip azimuth/dip. The lower hemisphere equal area projections show the shear zone orientation as measured in the field (solid) and the orientations of the shear zones after rotation (dashed) to the presumably original orientation. Black arrows represent the assumed shortening direction based on the rotation of the yellow arrows in the photograph (see text for details). Rotation is based on the rotation of the measured magmatic layering near the shear zone to that of the magmatic layering (magnitude of rotation given with each plot) in the western part of the study area, which presumably corresponds to the original orientation. As it is unknown whether rotation occurred in a clockwise (CW) or counter-clockwise (CCW) direction both rotations were performed and are shown as two separate projections. RP - rotation pole. The arrows show the shortening direction. a) Two intersecting shear zones with sinistral and normal-oblique (dextral component) offset, respectively. b) Photomosaic of two intersecting shear zones with dextral and sinistral offset, respectively.

(Fig. 7a–c).

Pl adjacent to the shear zone is locally fractured and the fractures are filled with fine-grained Amp. The fractures occur in two orientations, with the dominant set parallel to the shear zone boundary. These shear zone-parallel fractures are most abundant immediately adjacent to the shear zone (Fig. 6f). The fractured Pl is also characterized by patchy extinction under crossed-polarized light, and by finer Pl grains along grain boundaries and fractures.

The matrix of small-scale shear zones also contains Cpx-Pl symplectites as those of the foliated amphibolite. Bt typically occurs associated with the corona-type microstructures. As in the foliated amphibolites, Grt is inclusion-rich (see Sections 6 and 7) and commonly richer in inclusions toward the rim of the coronas.

#### 5.4. Massive amphibolites and retrogressed eclogites

Massive amphibolite is composed of the same mineral assemblage as the foliated amphibolite. It is typically coarser and non-foliated, although there are gradual transitions between weakly foliated and

strongly foliated amphibolites. Retrogressed eclogite is rare in the studied area. Throughout this contribution we refer to retrogressed eclogite only where the rocks have Omp preserved in the matrix. However, even in these rocks most Omp has been replaced by Cpx-Pl symplectites and Amp.

## 6. Garnet mineral chemistry and microstructures

Garnet is typically fractured and inclusion-rich. Inclusions of Amp, Qz, Cpx, epidote, apatite, rutile, and Fe-(Ti)-oxides occur, although typically not all present in the same grain. Optically and in BSE images Grt has the appearance of single crystals ranging in size from 0.2 to >5 mm. Grt phase boundaries vary from straight to irregular in small-scale shear zones. In the foliated amphibolite, phase boundaries are exclusively irregular, while retrogressed eclogite preserves dominantly straight grain boundaries.

The distribution of inclusions in Grt is typically heterogeneous, with inclusion-rich zones sharply bordering zones of no or few inclusions (Fig. 9a and 10). The included Cpx is either Omp (up to  $\sim$ Jd<sub>40</sub>), or

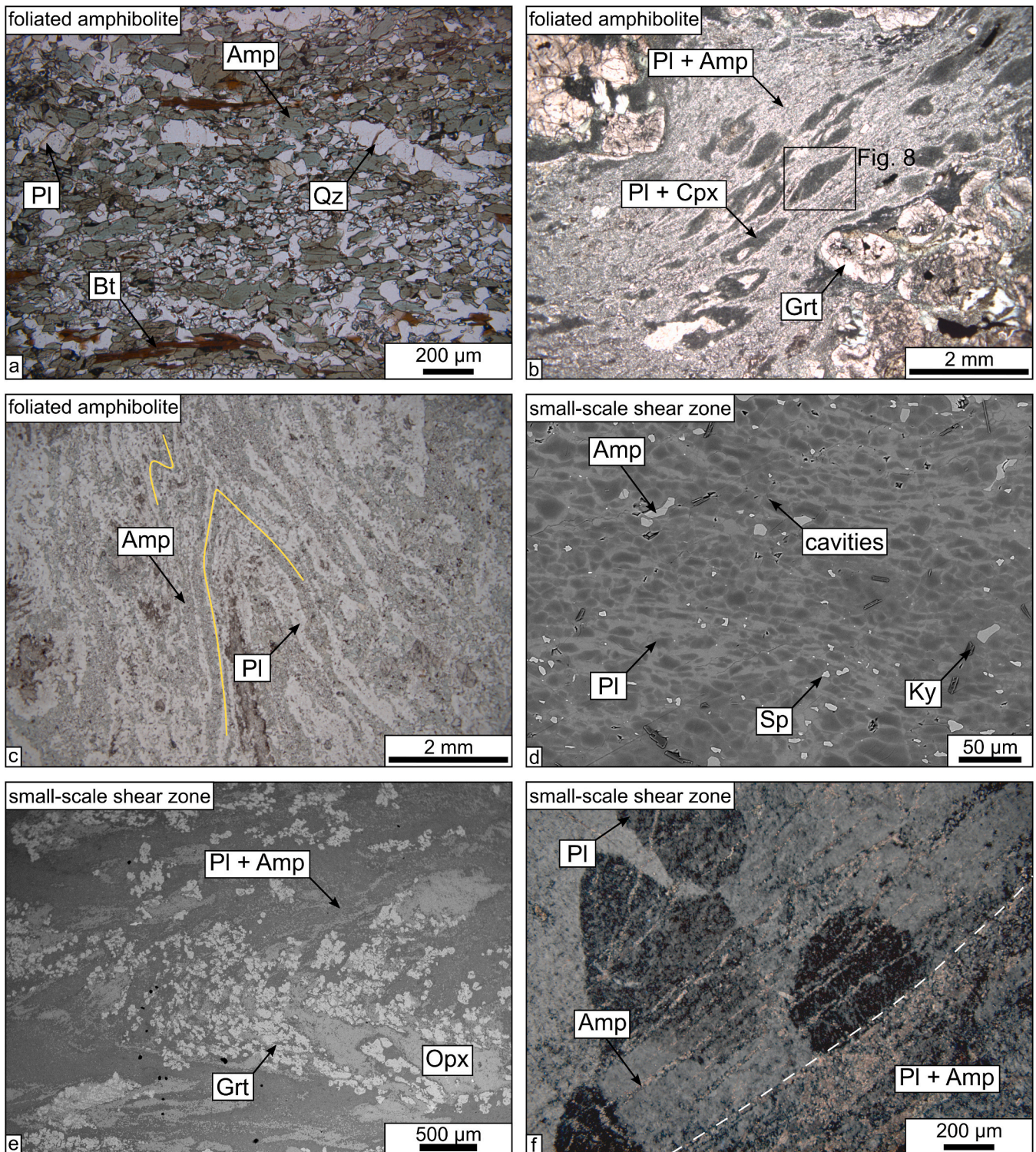


**Fig. 6.** Representative microstructures in the study area. a) Photomicrograph (plane-polarized light, PPL) showing the strongly developed SPO of Amp in the foliated amphibolite. b) Photomicrograph (PPL) of the foliated amphibolite with large Grt porphyroclasts and the Pl-Amp matrix wrapping around it. Dark material in the center of the image is Cpx-Pl symplectites after Omp. c) Photomicrograph (PPL) of the foliated amphibolite showing that the foliation formed by Amp and Pl is folded. d) BSE image of a small-scale shear zone showing Pl with inverse zoning (anorthite-rich rim surrounding albite-rich core; see Mukai et al., 2014) and cavities along grain boundaries. e) BSE image of a small-scale shear zone in gabbro. In this example Grt does not completely surround the Opx-porphyroclasts but occurs more chaotically distributed. Nucleation of Grt, however still occurs close to Opx. Grt in this sample does not contain Omp inclusions. f) Photomicrograph (cross-polarized light) of Pl adjacent to a small-scale shear zone showing microfractures lined by Amp.



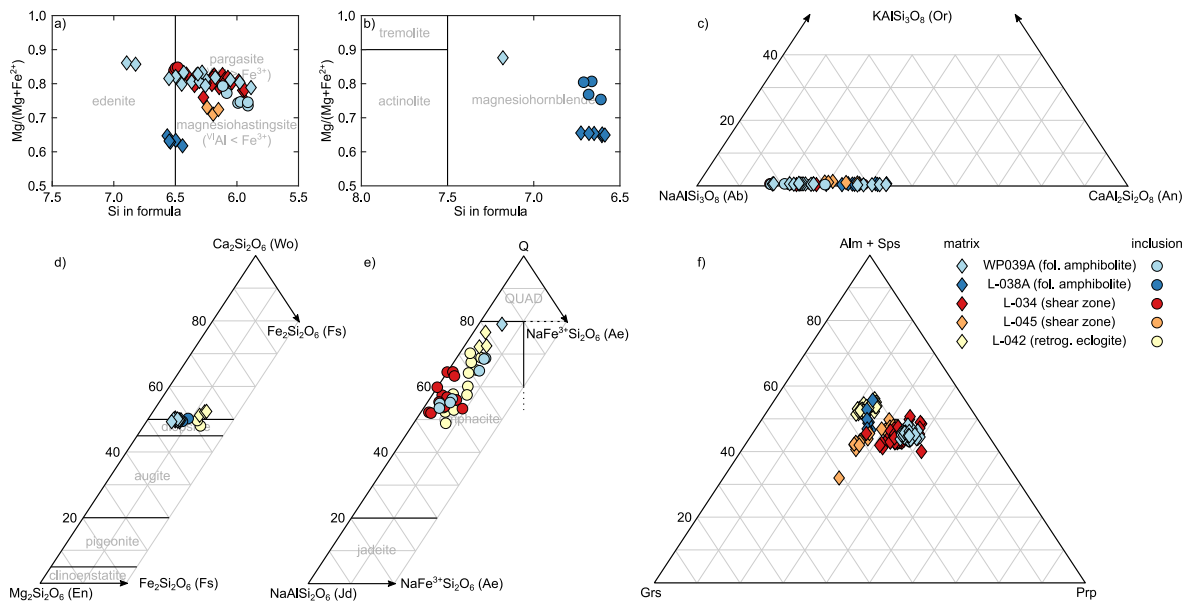


**Fig. 7.** Diagrams depicting variations in mineral chemistry from EMPA spot analysis of Amp (a, b), Pl (c), Cpx (d, e), and Grt (f). The legend on the right is valid for all diagrams. Fol. amphibolite - foliated amphibolite that forms the main shear zone. Shear zone refers to small-scale shear zones in the gabbro. Retrog. eclogite - retrogressed eclogite. Mineral formula calculation was done based on [Leake et al. \(1997\)](#) for Amp, [Morimoto \(1988\)](#) for Cpx and [Locock \(2008\)](#) for Grt. Pl analyses were normalized to 8 oxygens. Abbreviations in f: Alm - almandine; Sps - spessartine; Grs - grossular; Prp - pyrope.

diopside, depending on the sample (Fig. 7d and e). Inclusions of Amp and Pl have the same chemical composition as those in the matrix (Fig. 7a–c). Ky inclusions may define a SPO within Grt (Fig. 11a). In general, Grt with Omp inclusions is characterized by distinct Ca-richer cores (Fig. 9). In samples without Omp inclusions Grt may still have a Ca-richer core, but this is not always the case.

Qualitative mapping of element distributions reveals Mg zonation with a general core-to-rim relationship inverse to the Ca zoning. Zoning of Mg and Ca reveals several domains with higher Ca (and lower Mg) contents, specifically in samples from small-scale shear zones (Fig. 9a). Contrary to this, Mn is typically enriched in a continuous outer rim (Fig. 9b) in samples from small-scale shear zones and amphibolites. No Mn-rich rim was detected in the retrogressed eclogites (Fig. 9d). Transitions between compositional zones can be either sharp, especially in the retrogressed eclogites, or more commonly gradual. Variations in Grt composition are subtle (Fig. 7f) and most clearly visible in X-ray maps (Fig. 9).

## 7. Electron backscatter diffraction of garnet

EBSDF analysis from a small-scale shear zone reveals that Grt grains that appear homogeneous in BSE images are dissected by high angle boundaries (grain boundaries) typically with misorientations between 20 and 50° (Fig. 10). Misorientation profiles show sharp jumps across, and no evidence of distortion of the crystal lattice adjacent to the grain boundaries.

One grain of the Grt in Fig. 10 (blue-purple grain at the top) additionally displays a polygonized zone characterized by low angle boundaries, with misorientation angles dominantly <2°. Plotting of (110) of Grt (in the polygonized area) together with (001) of adjacent Bt shows that these poles are coincident.

## 8. Pressure-temperature estimates

Conventional geothermobarometry was performed for two samples of the foliated amphibolite based on EMPA spot analysis of Amp and Pl using (i) the geothermometer of [Holland and Blundy \(1994\)](#); thermometer B), based on element exchange between Pl and Amp; (ii) and the geobarometers of [Anderson and Smith \(1995\)](#) and [Molina et al. \(2015\)](#),

based on the Al content in Amp and the Pl-Amp Al-Si partitioning, respectively. Sites for analysis were chosen based on microstructural criteria that indicate equilibrium conditions, i.e., straight phase boundaries between Amp and Pl. The barometer by [Anderson and Smith \(1995\)](#) requires that  $Fe^{3+}/Fe^{tot} > 0.2$ , which is not always the case (see [Tables S1–S4](#)). The results are nevertheless reported, as there seems to be no systematic difference with respect to the analyses that fulfill this requirement. The spreadsheet of [Anderson et al. \(2008\)](#) was used for the calculation of the [Anderson and Smith \(1995\)](#) barometer and the [Holland and Blundy \(1994\)](#) thermometer.

The analyzed sample WP039A contains Omp inclusions in Grt and Cpx-Pl symplectites in the matrix. The P-T estimate yields  $701 \pm 38$  °C ([Holland and Blundy, 1994](#); reported as mean  $\pm 1$  standard deviation),  $8.5 \pm 1.2$  kbar ([Anderson and Smith, 1995](#)),  $11.2 \pm 0.7$  kbar ([Molina et al., 2015](#)). The analysis included Amp-Pl pairs within Cpx-Pl symplectites (see [Tables S1 and S2](#)), which yield consistently lower values than mineral pairs in the matrix ( $669 \pm 8$  °C,  $7.6 \pm 0.6$  kbar, and  $10.6 \pm 0.3$  kbar in the symplectite vs.  $728 \pm 31$  °C,  $9.2 \pm 1.0$  kbar, and  $11.7 \pm 0.3$  kbar in the matrix).

The sample L-038 contains diopside inclusions in Grt. The P-T estimate yields  $648 \pm 14$  °C ([Holland and Blundy, 1994](#)),  $7.1 \pm 0.6$  kbar ([Anderson and Smith, 1995](#)), and  $9.4 \pm 0.3$  kbar ([Molina et al., 2015](#)).

## 9. U-Pb zircon dating of pegmatites

U-Pb dating was performed on two pegmatite dykes that cross-cut the amphibolite foliation (locations in Fig. 3d). One of the dykes is weakly folded (RAM9; Fig. 2d), and the other is straight (RAM8). Both samples contain euhedral prismatic, clear to pink zircon crystals, generally fractured. Four analyses were obtained from sample RAM9 (Fig. 12a, Table S5). One of them is reversely discordant, presumably due to the presence of organic interferences while measuring. The other three data points are concordant and overlap defining an average  $^{206}Pb/^{238}U$  age of  $413.15 \pm 0.56$  Ma. Sample RAM8 yielded six data points that overlap within uncertainty and are concordant providing an average  $^{206}Pb/^{238}U$  age of  $412.66 \pm 0.40$  Ma (Fig. 12b, Table S5).

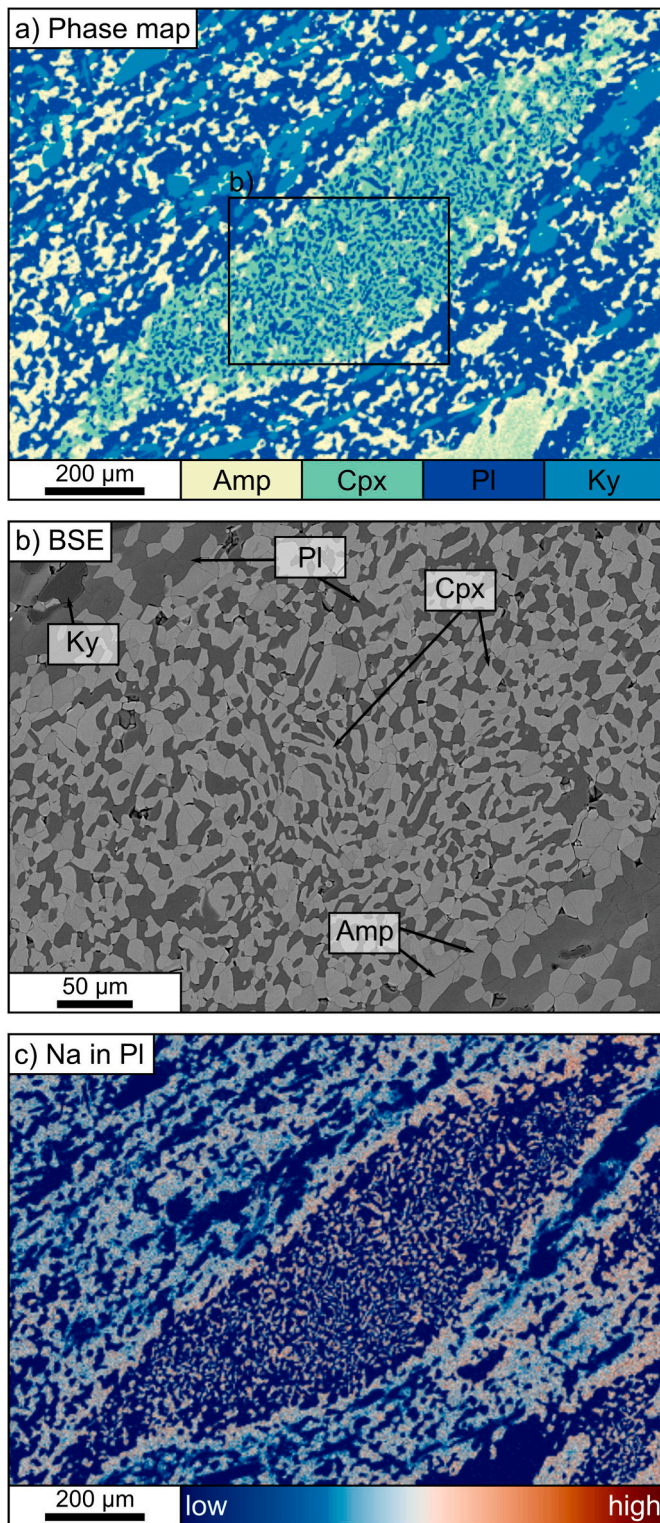


**Fig. 8.** Cpx-Pl symplectite after Omp. a) Phase map of a Cpx-Pl symplectite within a foliated amphibolite. Amp occurs rarely within the Cpx-Pl symplectite but rims the entire boundary between Cpx-Pl symplectite and matrix. b) BSE image of the center of the Cpx-Pl symplectite (see box in a for location). The center preserves a vermicular microstructure indicative of static retrogression. Only Cpx and Pl show this microstructure. c) SEM EDS map showing the relative distribution of Na in Pl.

## 10. Discussion

### 10.1. Metamorphic evolution at the Ramberg locality

The studied locality exposes a shear zone that preserves evidence of several stages of deformation and metamorphic re-equilibration (Figs. 13 and 14). The first stage is related to migmatization of the host rock (gabbro). Although there is no direct geochronological information, the gabbro likely belongs to the Paleoproterozoic rocks that were intruded by the AMCG suite between 1.9 and 1.7 Ga (Tveten, 1978; Corfu, 2004). Alternatively, the gabbro is part of the magmatic suite that intruded at that time which is supported by ages of inherited igneous zircon of  $\sim 1.8$  Ga from the eclogites (Jaranowski et al., 2023). Either way, the emplacement of nearby AMCG plutons may have led to migmatization of the host rock (Stage I in Fig. 14). We thus argue that the migmatitic fabric is genetically related to the emplacement of plutons within the lower crust, sometime before  $\sim 1.7$  Ga.

A second metamorphic stage is recorded by the occurrence of Omp inclusions in Grt (Stage II in Fig. 14) and of abundant Cpx-Pl symplectites that indicate the former presence of Omp within the matrix (Anderson and Moecher, 2007). Hence, these rocks experienced eclogite-facies conditions. Since this stage is only sparsely preserved, there is little structural control on the associated deformation features. However, the dominant trend of the main amphibolite foliation (containing Grt with Omp inclusions) and the older migmatite layering are parallel (Fig. 1c; Fig. 2f). Additionally, the eclogites from nearby localities in Vikten and Myrland (Markl and Bucher, 1997; Steltenpohl et al., 2011) are located along strike of this foliation. Therefore, we infer that eclogitization occurred along a zone that was structurally coincident with the overprinting amphibolite-facies shear zone and exploited the pre-existing magmatic/granulite-facies regional fabric. The occurrence of Omp inclusions in Grt (Fig. 11) and Cpx-Pl symplectites within small-scale shear zones, and the SPO of Ky inclusions in Grt (Fig. 11) indicate that deformation may have accompanied the eclogite-facies stage.

Analysis of Grt inclusion assemblages, mineral chemistry, and crystallographic data indicate that Grt nucleated at eclogite-facies conditions (Omp inclusions in Ca-richer Grt cores; Fig. 9; Fig. 11). Grt nucleation was followed by progressive growth. High-angle boundaries dissecting Grt with several cores are interpreted to result from coalescence of several Grt grains (e.g., Whitney et al., 2008). Likewise, the coincidence of Grt (110) and Bt (001) indicates epitaxial growth of Grt onto Bt (Fig. 10), and that the low-angle boundaries are not related to deformation (Spiess et al., 2007; Nagurney et al., 2021). The occurrence of parasitic Amp along the high-angle boundaries (Fig. 11) indicates that coalescence occurred after the end of the eclogite-facies event. Gradual changes in Grt composition provide evidence that some diffusional modification erased part of the growth zoning, making it difficult to verify the existence of an intermittent stage (e.g., resorption features; Giuntoli et al., 2018a). However, though dependent on bulk rock composition, Ca-content in Grt is pressure sensitive (e.g., Kretz, 1959; Uno et al., 2015; Baxter et al., 2017), and the core-to-rim zoning in Grt (Ca-richer to Ca-poorer; Fig. 9) is consistent with decompression during Grt growth.

The P-T conditions for the eclogitization process are difficult to assess due to the limited preservation of the eclogite assemblage. Previous studies have determined P-T conditions of 1.4–1.5 GPa and 540–680 °C (Markl and Bucher, 1997) and 2.5–2.8 GPa and  $\sim 650$  °C (Froitzheim et al., 2016). The uncertainty pertaining to the mineral assemblage at peak conditions precludes their determination by means of bulk rock thermodynamic calculations. This is complicated further, because none of the metamorphic events affected the entire rock volume, and the reaction volume is thus unknown.

Nevertheless, a minimum estimate of the P-T conditions can be obtained from the Cpx-Pl symplectites (after Omp). Anderson and Moecher (2007) have suggested that the breakdown of Omp occurs at higher

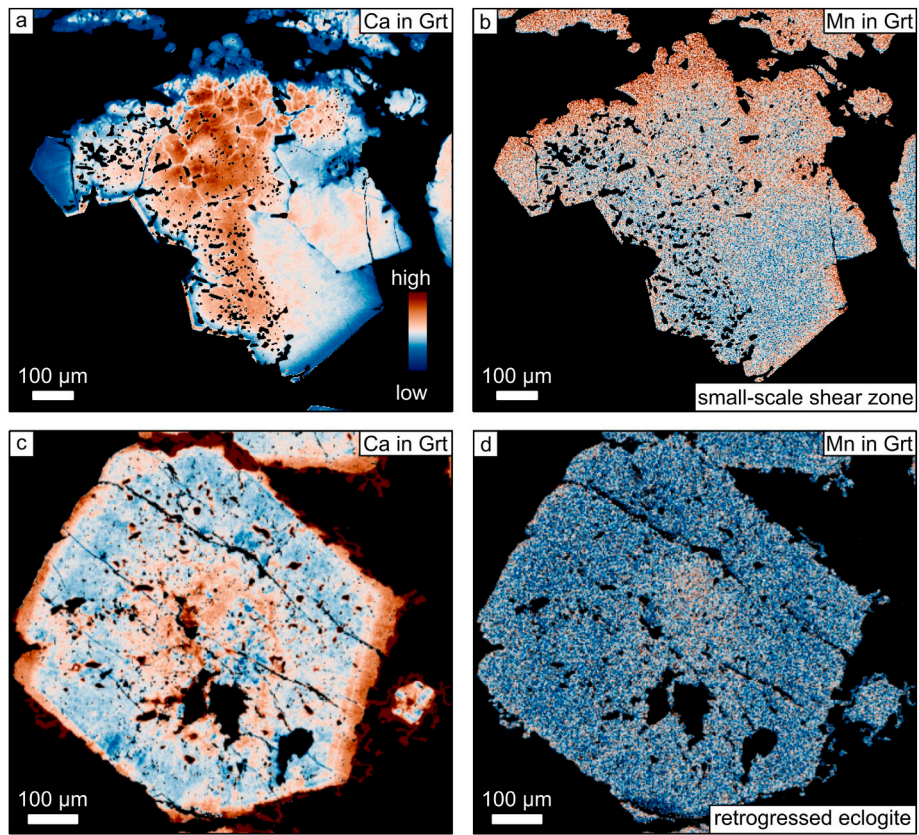


Fig. 9. Examples of variation in garnet composition. a, b) EMPA map of Ca and Mn, respectively, of a Grt from a small-scale shear zone. c, d) EMPA map of Ca and Mn, respectively, of a Grt from a retrogressed eclogite.

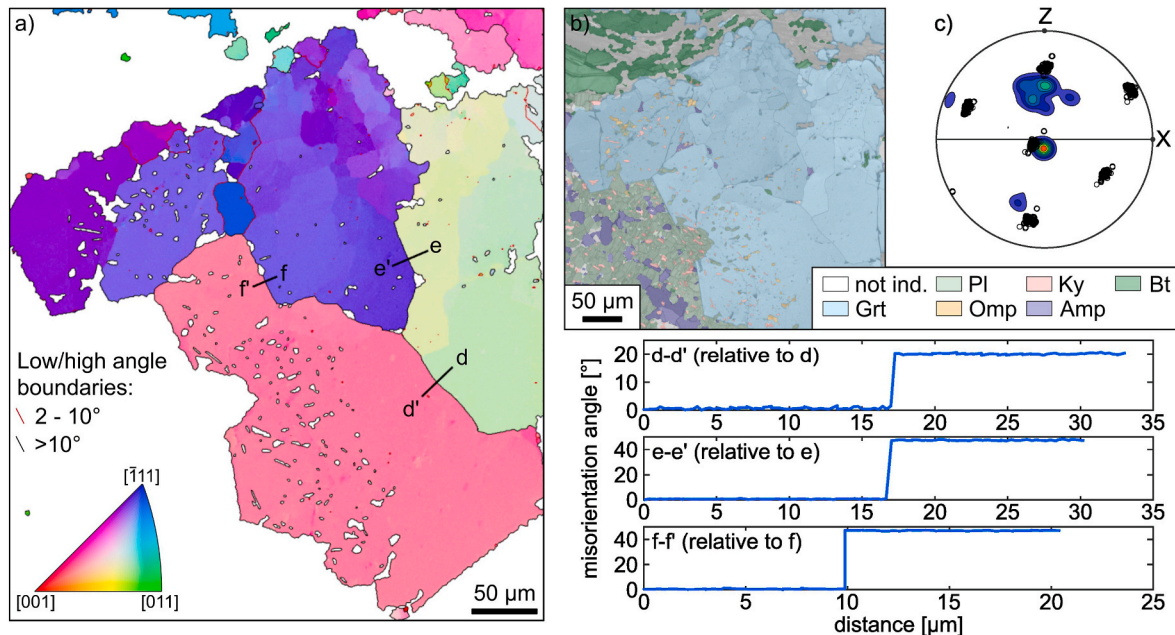
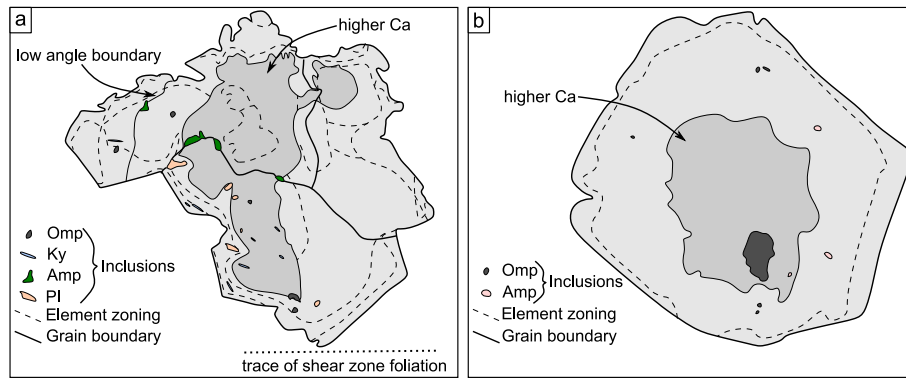


Fig. 10. Results of EBSD analysis the Grt shown in Fig. 9a and b. a) Inverse pole figure map (X-direction). b) Combined band contrast and phase map. c) Pole figure showing Bt (001) as contours and Grt (110) as open circles. X – lination, Z – pole to foliation. d-d', e-e', and f-f' correspond to the misorientation profiles shown in the lower right corner. All misorientation profiles show misorientation angles relative to the first point of the profile.

pressure for higher Jd contents. Additionally, the breakdown of Omp is considered to occur without significant element exchange with the surrounding rock (e.g., Anderson and Moecher, 2007; Martin, 2019), as is supported by the preservation of Cpx-Pl symplectites sharply

bordering the Amp-Pl matrix (Fig. 8). The composition locally available for the reaction is thus given by the composition of the Omp. We calculated the stability field of Omp for two compositions (Jd<sub>20</sub> and Jd<sub>40</sub>), corresponding to the lowest and highest Jd contents found for the



**Fig. 11.** Sketches illustrating key microstructural and chemical relationships of the Grt shown in Figs. 9 and 10. The Grt in (a) grew by coalescence of several Grt nuclei and has Omp inclusions in the cores and Amp occurring only along the grain boundaries. The Grt shown in b has concentric growth zoning with Omp inclusions in the core and mantle, and no inclusions of Amp. The dashed lines represent the position of zones interpreted from all available element maps (see Figs. S8 and S10).

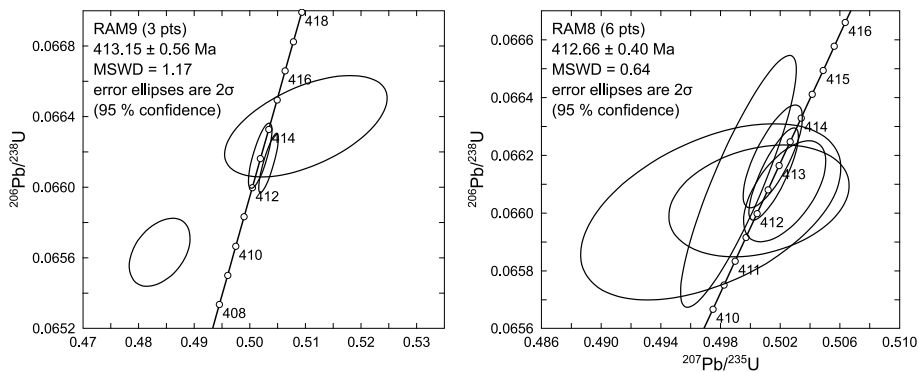


**Fig. 12.** Concordia diagram showing the zircon U-Pb data from two pegmatite dykes that cross-cut the amphibolite foliation of the main shear zone. The location of both dykes is shown in Fig. 3d. RAM9 was sampled from the dyke shown in Fig. 2d.

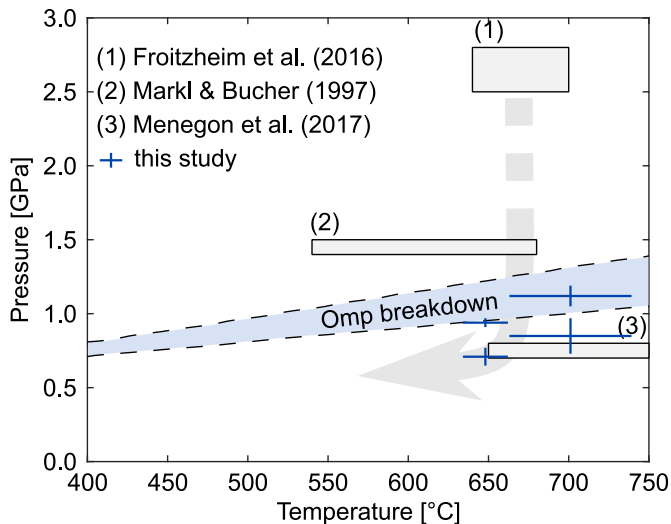


**Fig. 13.** Summary of published P-T conditions for the eclogite-facies (1, 2) and amphibolite-facies (3) metamorphism in Lofoten together with those from this study. The “Omp breakdown” field is defined by the stability of Omp with Jd<sub>40</sub> (top dashed line) and Jd<sub>20</sub> (bottom dashed line) as calculated using Thermolab (see text for details).

Omp inclusions in Grt (Fig. 7e). Our calculations suggest Omp breakdown between 1.3 and 0.9 GPa, assuming a temperature range of 640–700 °C (Fig. 13), and that reaction kinetics are sufficient. This

provides a lower bound to the eclogitization pressure of ~1.3 GPa.

The third stage that affected the rocks occurred at amphibolite-facies conditions of ~0.7–1.1 GPa and ~650–700 °C as estimated by geothermobarometry from Amp-Pl pairs (Fig. 13; Stage III in Fig. 14). Amphibolitization exploited the pre-existing composite (stage I and II) structural framework (Fig. 3).

The crenulation folds in the western part of the studied area with fold axial planes parallel to the main foliation indicate that sinistral shearing was accompanied by shortening perpendicular to the shear plane. This outcrop is located at the boundary of the main shear zone and the corresponding fold axes are shallowly plunging parallel to the stretching lineation in the shear zone (Fig. 3b and c). The folded mafic dyke (Fig. 2e) found in another location has a steeper fold axis (351/38). Shortening perpendicular to the shear plane with progressive steepening of fold axes is consistent with deformation in a transpressional shear zone (Treagus and Treagus, 1992; Fossen et al., 1994). The crenulation folds are interpreted as parasitic folds and the orientation of the foliation across the main shear zone is consistent with the entire section being affected by folding with a fold axial plane dipping steeply to the SE and with near horizontal fold axes (Fig. 3). This is supported by the  $\pi$ -circle reconstruction (Fig. 3b), although the scatter of the data is large, reflecting the changes in orientation as the foliation wraps around low-strain domains. However, parasitic folds were not observed further to the E. It is thus unclear if folding occurs localized, for example, along the shear zone boundary during incipient integration into the main shear zone, or if the entire section is folded.

Folded Amp and Pl layers seen in thin section (Fig. 6c) indicate that the rock had an amphibolite-facies mineral assemblage prior to folding, but also that this mineral assemblage remained stable during folding.

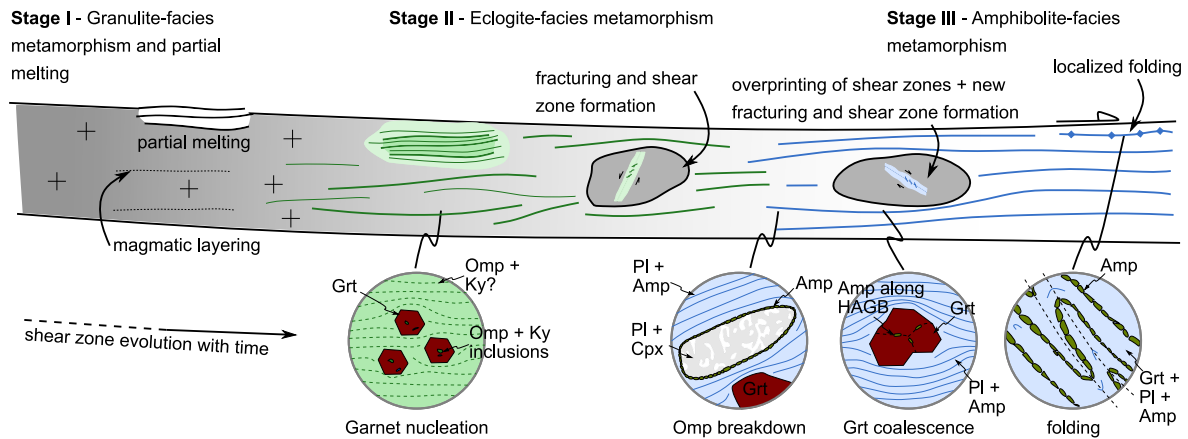


Fig. 14. Interpretative sketch showing the evolution of the Ramberg shear zone (see main text for details). HAGB – high-angle grain boundary.

Folding thus occurred during the amphibolite-facies stage. To interpret these observations in the context of large-scale folding of the entire section would require that the amphibolite-facies foliation was initially horizontal, which in turn suggests a switch in the kinematic framework. Alternatively, the variations in orientation of the main foliation reflects strain partitioning, as weak layers anastomose around stiff lenses (low-strain domains). In this case, internal localized folding is consistent with a transpressive regime, that may lead to the localized formation of folds without the need of invoking a change in the kinematic framework. Finally, the ages of pegmatite dykes that cross-cut the foliation indicate that deformation terminated at  $\sim 412$  Ma (Fig. 12).

The breakdown of Omp to Cpx-Pl symplectites is generally regarded as a static process (Anderson and Moecher, 2007) as is supported by the vermicular microstructure preserved in their core (Fig. 8). The granular microstructure along the rim and the elongation parallel to the amphibolite-facies foliation indicate grain growth and deformation. Cpx-Pl symplectites may have formed statically before the amphibolite-facies deformation or synkinematically. Both would be consistent with similar symplectic microstructures in granitoid mylonites, where myrmekites preserve their vermicular microstructure in the interior of K-feldspar porphyroclasts, while they recrystallize and deform along the mylonitic foliation (Menegon et al., 2006; Ceccato et al., 2018). Alternatively, Cpx-Pl symplectites may have preserved an Omp core after deformation, that subsequently retrogressed. We cannot distinguish conclusively between these alternatives, but the fact that the Cpx-Pl symplectites contain some Amp suggests that a fluid was involved and consumed during recrystallization. Because these Amp do not occur within the vermicular portion of the Cpx-Pl symplectites we favor static retrogression prior to deformation. The fact that P-T estimates from the symplectite are consistently lower than in the surrounding matrix may be evidence that Omp breakdown occurred late during decompression. Alternatively, these P-T conditions may record either late grain growth after the main deformation phase (Martin, 2019), or simply be caused by not fully established equilibrium between the analyzed Amp and Pl.

### 10.2. Implications for the position of the Lofoten block during the Caledonian collision

The position of the Lofoten block during the Caledonian collision is somewhat enigmatic as it occupies an internal position within the Caledonian orogen, but the metamorphic overprint is minor compared to, for example, the Western Gneiss Region (e.g., Labrousse et al., 2004; Hacker et al., 2010; Tamblin et al., 2022). It has been proposed that the Lofoten block was subducted to a depth of  $\sim 90$  km during the Scandian phase of the Caledonian collision (Froitzheim et al., 2016; Jaranowski et al., 2023). Three ages for eclogite-facies metamorphism have been published so far:  $478 \pm 41$  Ma, the lower intercept age of discordant

zircon U-Pb analyses (Steltenpohl et al., 2011),  $427 \pm 6$  Ma from concordant U-Pb analyses of metamorphic zircon (Jaranowski et al., 2023), and  $399 \pm 10$  Ma based on Grt Lu-Hf geochronology (Froitzheim et al., 2016). Our structural and microstructural observations combined with the ages of only weakly deformed pegmatite dykes provide conclusive evidence that the Lofoten block was at amphibolite-facies conditions at  $\sim 412$  Ma, and that the eclogite-facies event had already concluded at that time. The eclogite-facies event has thus occurred during early Scandian collision or before.

Given the structural framework of the Lofoten eclogites an alternative to deep subduction must be considered. The eclogites occur exclusively along a tabular pre-existing heterogeneity, i.e., a pre-existing fabric (Fig. 1). The remainder of the crustal section exposed in Lofoten dominantly preserves a granulite- or amphibolite-facies assemblage demonstrating that these rocks were unaffected by the eclogite-facies event, and remained dry and strong (e.g., Jackson et al., 2004). Considering that re-equilibration of dry rocks is inhibited by slow reaction kinetics (e.g., Austrheim, 1990; John and Schenk, 2003; Jackson et al., 2004; Jamtveit et al., 2019; Kaatz et al., 2021; Zertani et al., 2022) fluid infiltration is necessary to facilitate metamorphic reactions. The infiltration of fluids along a planar fabric would result in a weak tabular zone within otherwise dry and strong rocks. Such a setting is a prime candidate for deviations from lithostatic pressure conditions, i.e., overpressure (Mancktelow, 1993, 2008; Moulas et al., 2014, 2022). The magnitude of such pressure variations is beyond the scope of this study, however, Putnis et al. (2021) and Moulas et al. (2022) recently found that pressure excursions on the order of 0.5 GPa are realistic for hydrous shear zones hosted in otherwise dry and strong granulites. Eclogites localized in hydrated shear zones within granulitic gabbros elsewhere in Lofoten (Nusfjord West) were indeed interpreted as the result of local pressure variations caused by fluid-induced weakening (Jamtveit et al., 2019). Additionally, if the P-T results of Froitzheim et al. (2016) reflect isobaric conditions, isothermal decompression on the order of up to 1 GPa would be required, a circumstance that is increasingly attributed to possible excursions from isobaric pressure (e.g., Simon et al., 2023).

As a result, it is unclear how “deep” the Lofoten block was subducted. In either case our results conclusively place this section of lower crust at amphibolite-facies conditions during the Scandian phase of the Caledonian collision. Moreover, subhorizontal shortening in NW-SE direction as derived from our structural analysis (Fig. 3) is consistent with shortening during the Scandian phase of the Caledonian collision (e.g., Roberts, 2003; Jakob et al., 2019). We thus conclude that the amphibolite-facies event is related to (Scandian) Caledonian deformation.

### 10.3. Implications for the deformation of the continental crust

The multiphase sequence of deformation and metamorphism revealed by this study (Fig. 14) has significant implications for how the lower continental crust deforms during an orogeny, beyond the regional implications outlined above.

Various studies have shown that the dry, lower continental crust is unable to react (re-equilibrate) to changing P-T conditions, necessitating the addition of fluids to facilitate metamorphic re-equilibration (e.g., Austrheim, 1987; Wayte et al., 1989; Jamtveit et al., 2000; John and Schenk, 2003; Jackson et al., 2004; Jolivet et al., 2005; Jamtveit and Austrheim, 2010; Plümper et al., 2017; Centrella, 2019; Jamtveit et al., 2019; Zertani et al., 2019; Bras et al., 2021; Putnis et al., 2021; Rogowitz and Huet, 2021; Kaatz et al., 2022; Zertani et al., 2022; Baisset et al., 2023). At the same time, fluid infiltration may result in weakening of the crust and fluid pathways, which in turn, are influenced by pre-existing structural heterogeneities.

In the present case, primary lithological and structural variations provided pre-existing heterogeneities that significantly impacted the style of crustal deformation. These fabrics were formed >1.7 Ga ago and served to channelize metamorphism and deformation until the Caledonian collision at  $\geq 412$  Ma. During this time span of  $\sim 1.3$  Ga the fabric, initially formed by the migmatitic/magmatic layering, was re-used several times. Considering that re-equilibration required the addition of fluids, it follows that this layering channelized fluid flow (e.g., Oliver, 1996). The gabbros do not contain hydrous phases in significant proportions while the main shear zone is dominated by amphibole. It is thus evident that hydration accompanied deformation along the main shear zone.

At the same time, blocks of unaltered gabbro did not hydrate as they lacked the necessary fluid pathways. A dry lower crust is strong (Bürgmann and Dresen, 2008) and has negligible porosity and permeability (Manning and Ingebritsen, 1999). Several studies have consistently demonstrated that fracturing is the most efficient process to allow fluids to infiltrate lower-crustal rocks at amphibolite to eclogite-facies conditions, thereby facilitating metamorphic and rheological transformations (e.g., Pennacchioni and Mancktelow, 2013; Menegon et al., 2017; Leydier et al., 2019; Kaatz et al., 2021).

The formation of veins/fractures in low-strain domains associated with alteration halos (Fig. 4a and b) provides clear evidence that the rocks fractured and were infiltrated by fluids, and the formation of ductile shear zones along these veins/fractures (Fig. 4c and d) implies that fluid infiltration weakened the host rock (e.g., Mancktelow and Pennacchioni, 2005; Pennacchioni and Mancktelow, 2018; Kaatz et al., 2022). The observation that some of these small-scale shear zones contain Omp inclusions in Grt and Cpx-Pl symplectites, while others only preserve evidence of the amphibolite-facies event, indicates that brittle failure occurred both during the eclogite- and amphibolite-facies stages. Brittle deformation during the amphibolite-facies stage is further supported by fractures lined with Amp along the margin of small-scale shear zones (Fig. 6f; Okudaira et al., 2015). We thus conclude that brittle failure, fluid infiltration, and ductile deformation occurred cyclically during several stages of the deformation history.

Our reconstruction of shortening directions pertaining to intersecting shear zones may be reconcilable with the shortening direction of folding and thus with the Scandian collision (Fig. 5). However, as the data set is small, this is considered circumstantial evidence. The analyses do show, however, that the gabbro blocks were rotated during deformation and that such rigid-body rotation was punctuated by the formation of localized small-scale shear zones that nucleated on fractures. Deformation along the main ductile shear zone may have led to stress build-up in rigid blocks causing them to fracture (Hawemann et al., 2019; Campbell et al., 2020).

The Ramberg locality thus demonstrates the variability in deformation behavior of the continental crust. Rocks that were weak (hydrated) and heterogeneous were sheared and/or folded, while rocks that were

strong (dry) and homogeneous were fractured. This occurred cyclically throughout the deformation history. The studied locality therefore presents a prime example of how brittle and ductile deformation, fluid flow, and metamorphism interact along a heterogeneous shear zone in the deep crust over long periods of time.

## 11. Conclusions

Structural analysis of the Ramberg locality (Lofoten, northern Norway) reveals several features with implications both for the regional tectonic evolution of the Lofoten block and for the deformation behavior of the lower continental crust in general. From our analysis we draw the following conclusions:

1. The lower crust of the Lofoten block experienced eclogite-facies metamorphism. The zircon ages of  $\sim 412$ – $413$  Ma for the two pegmatite dykes (that cross-cut the foliation) preclude the possibility of a very late eclogitization, in the concluding stages of the Scandian event. Eclogitization must have occurred earlier during the Scandian collisional phase or before.
2. The style of deformation in the deep continental crust was controlled by pre-existing structural heterogeneities. During ongoing deformation, rock volumes that had pre-existing heterogeneities (e.g., foliation, layering) acted as fluid channels and were thus weakened making them more prone to ductile shearing, metamorphic reactions, and folding. Homogeneous rocks, however, remained dry and fractured, consequently creating new pathways for fluids to enter the rock volume. Such a deformation behavior occurred cyclically and at varying P-T conditions during the orogenic cycle.
3. Pre-defined structural heterogeneities can govern the deformation behavior and serve as fluid conduits over extremely long periods of time. In the case examined here, the structural framework was established during magmatic activity at  $\sim 1.7$  Ga, and the same framework was repeatedly re-used for  $\sim 1.3$  Ga.

## Author statement

**Sascha Zertani:** Conceptualization, Formal analysis, Investigation, Writing - Original Draft, Visualization, Funding acquisition. **Luca Menegon:** Conceptualization, Investigation, Writing - Review & Editing, Funding acquisition. **Giorgio Pennacchioni:** Investigation, Writing - Review & Editing. **Iris Buisman:** Investigation, Writing - Review & Editing. **Fernando Corfu:** Investigation, Writing - Review & Editing. **Bjørn Jamtveit:** Investigation, Writing - Review & Editing, Funding acquisition.

## Declaration of competing interest

The authors declare that they have no known competing financial interests or personal relationships that could have appeared to influence the work reported in this paper.

## Data availability

All data is provided in the manuscript and supplementary files. Raw data of EMPA maps is provided under <https://doi.org/10.5281/zenodo.8389143>.

## Acknowledgements

This research was supported by the Deutsche Forschungsgemeinschaft (DFG, German Research Foundation) grant 461241592 to SZ, ERC Advanced Grant no. 669972 'Disequilibrium Metamorphism' to BJ, the UK Natural Environment Research Council grant number NE/P001548/1 'The Geological Record of the Earthquake Cycle in the Lower Crust' to LM, Research Council of Norway FRIPRO

Grant no. 334965 'CONTINENT' to LM, and the European Union's Horizon 2020 Research and Innovation Programme under grant agreement No 101005611 for Transnational Access conducted at the Department of Earth Sciences, University of Cambridge. The Research Council of Norway is acknowledged for support to the Goldschmidt Laboratory national infrastructure (project number 295894). Holger Stünitz is thanked for introducing LM to the field area and for discussions. Stephen Michalchuk and Benoit Cordonnier are thanked for discussions in the field. Kristina Dunkel is acknowledged for providing the locations of the pegmatite dykes and comments on an earlier version of the manuscript. Siri Simonsen and Muriel Erambert are thanked for help during SEM and EMPA sessions. Three anonymous reviewers are acknowledged for their constructive reviews, as is Jianhua Li for editorial handling.

## Appendix A. Supplementary data

Supplementary data to this article can be found online at <https://doi.org/10.1016/j.jsg.2023.104960>.

## References

- Allmendinger, R.W., Cardozo, N., Fisher, D.M., 2011. *Structural Geology Algorithms: Vectors and Tensors*. Cambridge University Press, Cambridge.
- Andersen, T.B., Jamtveit, B., Dewey, J.F., Swenson, E., 1991. Subduction and exhumation of continental crust: major mechanisms during continent-continent collision and orogenic extensional collapse, a model based on the south Norwegian Caledonides. *Terra. Nova* 3, 303–310. <https://doi.org/10.1111/j.1365-3121.1991.tb00148.x>.
- Anderson, E.D., Moecher, D.P., 2007. Omphacite breakdown reactions and relation to eclogite exhumation rates. *Contrib. Mineral. Petrol.* 154, 253–277. <https://doi.org/10.1007/s00410-007-0192-x>.
- Anderson, J.L., Barth, A.P., Wooden, J.L., Mazdab, F., 2008. Thermometers and thermobarometers in granitic systems. *Rev. Mineral. Geochem.* 69, 121–142. <https://doi.org/10.2138/rmg.2008.69.4>.
- Anderson, J.L., Smith, D.R., 1995. The effects of temperature and fO<sub>2</sub> on the Al-hornblende barometer. *Am. Mineral.* 80, 549–559. <https://doi.org/10.2138/am-1995-5-614>.
- Austrheim, H., 1987. Eclogitization of lower crustal granulites by fluid migration through shear zones. *Earth Planet Sci. Lett.* 81, 221–232. [https://doi.org/10.1016/0012-821X\(87\)90158-0](https://doi.org/10.1016/0012-821X(87)90158-0).
- Austrheim, H., 1990. The granulite-eclogite facies transition: a comparison of experimental work and a natural occurrence in the Bergen Arcs, western Norway. *Lithos* 25, 163–169. [https://doi.org/10.1016/0024-4937\(90\)90012-z](https://doi.org/10.1016/0024-4937(90)90012-z).
- Bachmann, F., Hielscher, R., Schaeben, H., 2010. Texture analysis with MTEX—free and open source software toolbox. *Solid State Phenom.* 160, 63–68.
- Baïssset, M., Labrousse, L., Yamato, P., Schubnel, A., 2023. Twinning and partial melting as early weakening processes in plagioclase at high pressure: insights from Holsnøy (Scandinavian Caledonides, Norway). *Contrib. Mineral. Petrol.* 178, 19. <https://doi.org/10.1007/s00410-023-01998-x>.
- Baxter, E.F., Caddick, M.J., Dragovic, B., 2017. Garnet: a rock-forming mineral petrochronometer. *Rev. Mineral. Geochem.* 83, 469–533. <https://doi.org/10.2138/rmg.2017.83.15>.
- Bras, E., Baïssset, M., Yamato, P., Labrousse, L., 2021. Transient weakening during the granulite to eclogite transformation within hydrous shear zones (Holsnøy, Norway). *Tectonophysics* 819, 229026. <https://doi.org/10.1016/j.tecto.2021.229026>.
- Bürgmann, R., Dresen, G., 2008. Rheology of the lower crust and upper mantle: evidence from rock mechanics, geodesy, and field observations. *Annu. Rev. Earth Planet Sci.* 36, 531–567. <https://doi.org/10.1146/annurev.earth.36.031207.124326>.
- Campbell, L.R., Menegon, L., 2019. Transient high strain rate during localized viscous creep in the dry lower continental crust (Lofoten, Norway). *J. Geophys. Res. Solid Earth* 124, 10240–10260. <https://doi.org/10.1029/2019jb018052>.
- Campbell, L.R., Menegon, L., 2022. High stress deformation and short-term thermal pulse preserved in pyroxene microstructures from exhumed lower crustal seismogenic faults (Lofoten, Norway). *J. Geophys. Res. Solid Earth* 127, e2021JB023616. <https://doi.org/10.1029/2021JB023616>.
- Campbell, L.R., Menegon, L., Fagereng, Å., Pennacchioni, G., 2020. Earthquake nucleation in the lower crust by local stress amplification. *Nat. Commun.* 11, 1322. <https://doi.org/10.1038/s41467-020-15150-x>.
- Ceccato, A., Menegon, L., Pennacchioni, G., Morales, L.F.G., 2018. Myrmekite and strain weakening in granitoid mylonites. *Solid Earth* 9, 1399–1419. <https://doi.org/10.5194/se-9-1399-2018>.
- Ceccato, A., Menegon, L., Warren, C.J., Halton, A.M., 2020. Structural and metamorphic inheritance controls strain partitioning during orogenic shortening (Kalak Nappe Complex, Norwegian Caledonides). *J. Struct. Geol.* 136, 104057. <https://doi.org/10.1016/j.jsg.2020.104057>.
- Centrella, S., 2019. The Granulite- to Eclogite- and Amphibolite-Facies Transition: A Volume and Mass Transfer Study in the Lindås Nappe, Bergen Arcs, West Norway, vol. 478. Geological Society, London, Special Publications, pp. 241–264. <https://doi.org/10.1144/SP478.9>.
- Corfu, F., 2004. U–Pb age, setting and tectonic significance of the Anorthosite–Mangerite–Charnockite–Granite Suite, Lofoten–Vesterålen, Norway. *J. Petrol.* 45, 1799–1819. <https://doi.org/10.1093/petrology/egh034>.
- Corvò, S., Maino, M., Piazzolo, S., Seno, S., Langone, A., 2022. Role of inherited compositional and structural heterogeneity in shear zone development at mid-low levels of the continental crust (the Anzola shear zone; Ivrea-Verbano Zone, Southern Alps). *Lithos* 422–423, 106745. <https://doi.org/10.1016/j.lithos.2022.106745>.
- Cramer, F., 2018. Scientific colour-maps. Zenodo 10.
- Dunkel, K.G., Zhong, X., Arnestad, P.F., Valen, L.V., Jamtveit, B., 2021. High transient stress in the lower crust: evidence from dry pseudotachylytes in granulites, Lofoten Archipelago, northern Norway. *Geology* 49, 135–139. <https://doi.org/10.1130/G48002.1>.
- Fossen, H., Tikoff, B., Teyssier, C., 1994. Strain modeling of transpressional and transtensional deformation. *Nor. Geol. Tidsskr.* 74, 134–145.
- Froitzheim, N., Miladinova, I., Janák, M., Kullerød, K., Ravna, E.K., Majka, J., Fonseca, R. O.C., Münker, C., Nagel, T.J., 2016. Devonian subduction and syn-collisional exhumation of continental crust in Lofoten, Norway. *Geology* 44, 223–226. <https://doi.org/10.1130/g37545.1>.
- Fussey, F., Regenaier-Lieb, K., Liu, J., Hough, R.M., De Carlo, F., 2009. Creep cavitation can establish a dynamic granular fluid pump in ductile shear zones. *Nature* 459, 974–977. <https://doi.org/10.1038/nature08051>.
- Giuntoli, F., Lanari, P., Engi, M., 2018a. Deeply subducted continental fragments - Part 1: fracturing, dissolution-precipitation, and diffusion processes recorded by garnet textures of the central Sesia Zone (western Italian Alps). *Solid Earth* 9, 167–189. <https://doi.org/10.5194/se-9-167-2018>.
- Giuntoli, F., Menegon, L., Warren, C.J., 2018b. Replacement reactions and deformation by dissolution and precipitation processes in amphibolites. *J. Metamorph. Geol.* 36, 1263–1286. <https://doi.org/10.1111/jmg.12445>.
- Green, E., Holland, T., Powell, R., 2007. An order-disorder model for omphacitic pyroxenes in the system jadeite-diopside-hedenbergite-acmite, with applications to eclogitic rocks. *Am. Mineral.* 92, 1181–1189. <https://doi.org/10.2138/am.2007.2401>.
- Griffin, W.L., Taylor, P.N., Hakkinen, J.W., Heier, K.S., Iden, I.K., Krogh, E.J., Malm, O., Olsen, K.I., Ormaasen, D.E., Tveten, E., 1978. Archaean and Proterozoic crustal evolution in Lofoten–Vesterålen, N Norway. *J. Geol. Soc.* 135, 629–647. <https://doi.org/10.1144/gsjgs.135.6.0629>.
- Hacker, B.R., Andersen, T.B., Johnston, S., Kylander-Clark, A.R.C., Peterman, E.M., Walsh, E.O., Young, D., 2010. High-temperature deformation during continental-margin subduction & exhumation: the ultrahigh-pressure Western Gneiss Region of Norway. *Tectonophysics* 480, 149–171. <https://doi.org/10.1016/j.tecto.2009.08.012>.
- Hawemann, F., Mancktelow, N.S., Pennacchioni, G., Wex, S., Camacho, A., 2019. Weak and slow, strong and fast: how shear zones evolve in a dry continental crust (Musgrave ranges, Central Australia). *J. Geophys. Res. Solid Earth* 124, 219–240. <https://doi.org/10.1029/2018JB016559>.
- Holland, T., Blundy, J., 1994. Non-ideal interactions in calcic amphiboles and their bearing on amphibole-plagioclase thermometry. *Contrib. Mineral. Petrol.* 116, 433–447. <https://doi.org/10.1007/BF00310910>.
- Holland, T., Powell, R., 2003. Activity–composition relations for phases in petrological calculations: an asymmetric multicomponent formulation. *Contrib. Mineral. Petrol.* 145, 492–501. <https://doi.org/10.1007/s00410-003-0464-z>.
- Holland, T.J.B., Powell, R., 1998. An internally consistent thermodynamic data set for phases of petrological interest. *J. Metamorph. Geol.* 16, 309–343. <https://doi.org/10.1111/j.1525-1314.1998.00140.x>.
- Incel, S., Renner, J., Jamtveit, B., 2020. Evolution of brittle structures in plagioclase-rich rocks at high-pressure and high-temperature conditions – Linking laboratory results to field observations. *G-cubed* 21, e2020GC009028. <https://doi.org/10.1029/2020gc009028>.
- Jackson, J.A., Austrheim, H., McKenzie, D., Priestley, K., 2004. Metastability, mechanical strength, and the support of mountain belts. *Geology* 32, 625–628. <https://doi.org/10.1130/g20397.1>.
- Jaffey, A.H., Flynn, K.F., Glendenin, L.E., Bentley, W.C., Essling, A.M., 1971. Precision measurement of half-lives and specific activities of <sup>235</sup>U and <sup>238</sup>U. *Phys. Rev. C* 4, 1889–1906. <https://doi.org/10.1103/PhysRevC.4.1889>.
- Jakob, J., Andersen, T.B., Kjøl, H.J., 2019. A review and reinterpretation of the architecture of the South and South-Central Scandinavian Caledonides—a magma-poor to magma-rich transition and the significance of the reactivation of rift inherited structures. *Earth Sci. Res.* 192, 513–528. <https://doi.org/10.1016/j.earscirev.2019.01.004>.
- Jamtveit, B., Austrheim, H., Malthe-Sørensen, A., 2000. Accelerated hydration of the Earth's deep crust induced by stress perturbations. *Nature* 408, 75–78. <https://doi.org/10.1038/35040537>.
- Jamtveit, B., Austrheim, H., 2010. Metamorphism: the role of fluids. *Elements* 6, 153–158. <https://doi.org/10.2113/gselements.6.3.153>.
- Jamtveit, B., Bucher-Nurminen, K., Austrheim, H., 1990. Fluid controlled eclogitization of granulites in deep crustal shear zones, Bergen arcs, Western Norway. *Contrib. Mineral. Petrol.* 104, 184–193. <https://doi.org/10.1007/bf00306442>.
- Jamtveit, B., Petley-Ragan, A., Incel, S., Dunkel, K.G., Aupart, C., Austrheim, H., Corfu, F., Menegon, L., Renard, F., 2019. The effects of earthquakes and fluids on the metamorphism of the lower continental crust. *J. Geophys. Res. Solid Earth* 124, 7725–7755. <https://doi.org/10.1029/2018jb016461>.
- Jaranowski, M., Budzyń, B., Barnes, C.J., Majka, J., Sláma, J., Kozub-Budzyń, G.A., Kościńska, K., 2023. U–Pb and trace element zircon and apatite petrochronology of eclogites from the Scandinavian Caledonides. *Contrib. Mineral. Petrol.* 178, 47. <https://doi.org/10.1007/s00410-023-02029-5>.

- John, T., Schenk, V., 2003. Partial eclogitisation of gabbroic rocks in a late Precambrian subduction zone (Zambia): prograde metamorphism triggered by fluid infiltration. *Contrib. Mineral. Petrol.* 146, 174–191. <https://doi.org/10.1007/s00410-003-0492-8>.
- Jolivet, L., Raimbourg, H., Labrousse, L., Avigad, D., Leroy, Y., Austrheim, H., Andersen, T.B., 2005. Softening triggered by eclogitization, the first step toward exhumation during continental subduction. *Earth Planet. Sci. Lett.* 237, 532–547. <https://doi.org/10.1016/j.epsl.2005.06.047>.
- Kaatz, L., Reynes, J., Hermann, J., John, T., 2022. How fluid infiltrates dry crustal rocks during progressive eclogitization and shear zone formation: insights from H<sub>2</sub>O contents in nominally anhydrous minerals. *Contrib. Mineral. Petrol.* 177, 72. <https://doi.org/10.1007/s00410-022-01938-1>.
- Kaatz, L., Zertani, S., Moulas, E., John, T., Labrousse, L., Schmalholz, S.M., Andersen, T. B., 2021. Widening of hydrous shear zones during incipient eclogitization of metastable dry and rigid lower crust – Holsnøy, Western Norway. *Tectonics* 40, e2020TC006572. <https://doi.org/10.1029/2020TC006572>.
- Kretz, R., 1959. Chemical study of garnet, Biotite, and hornblende from gneisses of Southwestern Quebec, with emphasis on distribution of elements in coexisting minerals. *J. Geol.* 67, 371–402. <https://doi.org/10.1086/626594>.
- Krogh, T.E., 1973. A low-contamination method for hydrothermal decomposition of zircon and extraction of U and Pb for isotopic age determinations. *Geochem. Cosmochim. Acta* 37, 485–494. [https://doi.org/10.1016/0016-7037\(73\)90213-5](https://doi.org/10.1016/0016-7037(73)90213-5).
- Kullerød, K., Flaatt, K., Davidsen, B., 2001. High-pressure fluid–rock reactions involving Cl-bearing fluids in lower-crustal ductile shear zones of the Flakstadøy Basic Complex, Lofoten, Norway. *J. Petrol.* 42, 1349–1372. <https://doi.org/10.1093/ptrology/42.7.1349>.
- Labrousse, L., Jolivet, L., Andersen, T.B., Agard, P., Hébert, R., Maluski, H., Schärer, U., Whitney, D.L., Teyssier, C., Siddoway, C.S., 2004. Pressure-temperature-time deformation history of the exhumation of ultra-high pressure rocks in the Western Gneiss Region, Norway. In: Whitney, D.L., Teyssier, C., Siddoway, C.S. (Eds.), *Gneiss Domes in Orogeny*. Geological Society of America, pp. 155–183.
- Leake, B.E., Woolley, A.R., Arps, C.E., Birch, W.D., Gilbert, M.C., Grice, J.D., Hawthorne, F.C., Kato, A., Kisch, H.J., Krivovichev, V.G.J.M.M., 1997. Nomenclature of amphiboles; report of the Subcommittee on amphiboles of the international mineralogical association commission on new minerals and mineral names. *Can. Mineral.* 35, 219–246.
- Leydier, T., Goncalves, P., Lanari, P., Oliot, E., 2019. On the petrology of brittle precursors of shear zones – an expression of concomitant brittle deformation and fluid–rock interactions in the ‘ductile’ continental crust? *J. Metamorph. Geol.* 37, 1129–1149. <https://doi.org/10.1111/jmg.12504>.
- Locock, A.J., 2008. An Excel spreadsheet to recast analyses of garnet into end-member components, and a synopsis of the crystal chemistry of natural silicate garnets. *Comput. Geosci.* 34, 1769–1780. <https://doi.org/10.1016/j.cageo.2007.12.013>.
- Ludwig, K., 2009. *Isoplot 4.1. A Geochronological Toolkit for Microsoft Excel*, vol. 4. *Geochronology Center Special Publications*.
- Mancktelow, N.S., 1993. Tectonic overpressure in competent mafic layers and the development of isolated eclogites. *J. Metamorph. Geol.* 11, 801–812. <https://doi.org/10.1111/j.1525-1314.1993.tb00190.x>.
- Mancktelow, N.S., 2008. Tectonic pressure: theoretical concepts and modelled examples. *Lithos* 103, 149–177. <https://doi.org/10.1016/j.lithos.2007.09.013>.
- Mancktelow, N.S., Pennacchioni, G., 2005. The control of precursor brittle fracture and fluid–rock interaction on the development of single and paired ductile shear zones. *J. Struct. Geol.* 27, 645–661. <https://doi.org/10.1016/j.jsg.2004.12.001>.
- Manning, C.E., Ingebritsen, S.E., 1999. Permeability of the continental crust: implications of geothermal data and metamorphic systems. *Rev. Geophys.* 37, 127–150. <https://doi.org/10.1029/1998rg900002>.
- Markl, G., Bucher, K., 1997. Proterozoic eclogites from the Lofoten islands, northern Norway. *Lithos* 42, 15–35. [https://doi.org/10.1016/S0024-4937\(97\)00034-0](https://doi.org/10.1016/S0024-4937(97)00034-0).
- Markl, G., Frost, B.R., Bucher, K., 1998. The origin of anorthositic and related rocks from the Lofoten islands, northern Norway: I. Field relations and estimation of intrinsic variables. *J. Petrol.* 39, 1425–1452. <https://doi.org/10.1093/ptrology/39.8.1425>.
- Martin, C., 2019. P-T Conditions of Symplectite Formation in the Eclogites from the Western Gneiss Region (Norway), vol. 478. Geological Society, London, Special Publications, pp. 197–216. <https://doi.org/10.1144/SP478.18>.
- Mattinson, J., 2005. Zircon U-Pb chemical abrasion (CA-TIMS) method: combined annealing and multistep partial dissolution analysis for improved precision and accuracy of zircon ages. *Chem. Geol.* 220, 47–66.
- McKenzie, D., Jackson, J., 2002. Conditions for flow in the continental crust. *Tectonics* 21 (6), 1055. <https://doi.org/10.1029/2002TC001394>.
- Menegon, L., Campbell, L., Mancktelow, N., Camacho, A., Wex, S., Papa, S., Toffol, G., Pennacchioni, G., 2021. The earthquake cycle in the dry lower continental crust: insights from two deeply exhumed terranes (Musgrave Ranges, Australia and Lofoten, Norway). *Philosoph. Trans. Royal Soc. A* 379, 20190416. <https://doi.org/10.1098/rsta.2019.0416>.
- Menegon, L., Fusses, F., Stünitz, H., Xiao, X., 2015. Creep cavitation bands control porosity and fluid flow in lower crustal shear zones. *Geology* 43, 227–230. <https://doi.org/10.1130/G36307.1>.
- Menegon, L., Pennacchioni, G., Malaspina, N., Harris, K., Wood, E., 2017. Earthquakes as precursors of ductile shear zones in the dry and strong lower crust. *G-cubed* 18, 4356–4374. <https://doi.org/10.1002/2017GC007189>.
- Menegon, L., Pennacchioni, G., Stünitz, H., 2006. Nucleation and growth of myrmekite during ductile shear deformation in metagranites. *J. Metamorph. Geol.* 24, 553–568. <https://doi.org/10.1111/j.1525-1314.2006.00654.x>.
- Michalchuk, S.P., Zertani, S., Renard, F., Fusses, F., Chogani, A., Plümper, O., Menegon, L., 2023. Dynamic evolution of porosity in lower-crustal faults during the earthquake cycle. *J. Geophys. Res. Solid Earth* 128, e2023JB026809. <https://doi.org/10.1029/2023JB026809>.
- Molina, J.F., Moreno, J.A., Castro, A., Rodríguez, C., Fershtater, G.B., 2015. Calcic amphibole thermobarometry in metamorphic and igneous rocks: new calibrations based on plagioclase/amphibole Al-Si partitioning and amphibole/liquid Mg partitioning. *Lithos* 232, 286–305. <https://doi.org/10.1016/j.lithos.2015.06.027>.
- Molli, G., Tribuzio, R., Marquer, D., 2006. Deformation and metamorphism at the eastern border of the Tenda Massif (NE Corsica): a record of subduction and exhumation of continental crust. *J. Struct. Geol.* 28, 1748–1766. <https://doi.org/10.1016/j.jsg.2006.06.018>.
- Morimoto, N., 1988. Nomenclature of pyroxenes. *Mineral. Petrol.* 39, 55–76. <https://doi.org/10.1007/bf01226262>.
- Moulas, E., Burg, J.-P., Podladchikov, Y., 2014. Stress field associated with elliptical inclusions in a deforming matrix: mathematical model and implications for tectonic overpressure in the lithosphere. *Tectonophysics* 631, 37–49. <https://doi.org/10.1016/j.tecto.2014.05.004>.
- Moulas, E., Kaus, B., Jamtveit, B., 2022. Dynamic pressure variations in the lower crust caused by localized fluid-induced weakening. *Commun. Earth Environ.* 3, 157. <https://doi.org/10.1038/s43247-022-00478-7>.
- Mukai, H., Austrheim, H., Putnis, C.V., Putnis, A., 2014. Textural evolution of plagioclase feldspar across a shear zone: implications for deformation mechanism and rock strength. *J. Petrol.* 55, 1457–1477. <https://doi.org/10.1093/ptrology/egu030>.
- Nagurney, A.B., Caddick, M.J., Pattison, D.R.M., Michel, F.M., 2021. Preferred orientations of garnet porphyroblasts reveal previously cryptic templating during nucleation. *Sci. Rep.* 11, 6869. <https://doi.org/10.1038/s41598-021-85525-7>.
- Okudaira, T., Jerábek, P., Stünitz, H., Fusses, F., 2015. High-temperature fracturing and subsequent grain-size-sensitive creep in lower crustal gabbros: evidence for coseismic loading followed by creep during decaying stress in the lower crust? *J. Geophys. Res. Solid Earth* 120, 3119–3141. <https://doi.org/10.1002/2014JB011708>.
- Oliver, N.H.S., 1996. Review and classification of structural controls on fluid flow during regional metamorphism. *J. Metamorph. Geol.* 14, 477–492. <https://doi.org/10.1046/j.1525-1314.1996.00347.x>.
- Papa, S., Pennacchioni, G., Menegon, L., Thielmann, M., 2020. High-stress creep preceding coseismic rupturing in amphibolite-facies ultramylonites. *Earth Planet. Sci. Lett.* 541, 116260. <https://doi.org/10.1016/j.epsl.2020.116260>.
- Pennacchioni, G., 2005. Control of the geometry of precursor brittle structures on the type of ductile shear zone in the Adamello tonalites, Southern Alps (Italy). *J. Struct. Geol.* 27, 627–644. <https://doi.org/10.1016/j.jsg.2004.11.008>.
- Pennacchioni, G., Mancktelow, N.S., 2007. Nucleation and initial growth of a shear zone network within compositionally and structurally heterogeneous granitoids under amphibolite facies conditions. *J. Struct. Geol.* 29, 1757–1780. <https://doi.org/10.1016/j.jsg.2007.06.002>.
- Pennacchioni, G., Mancktelow, N.S., 2013. Initiation and growth of strike-slip faults within intact metagranitoid (Neves area, eastern Alps, Italy). *GSA Bulletin* 125, 1468–1483. <https://doi.org/10.1130/B30832.1>.
- Pennacchioni, G., Mancktelow, N.S., 2018. Small-scale ductile shear zones: neither extending, nor thickening, nor narrowing. *Earth Sci. Rev.* 184, 1–12. <https://doi.org/10.1016/j.earscirev.2018.06.004>.
- Plümper, O., Botan, A., Los, C., Liu, Y., Malthe-Sørensen, A., Jamtveit, B., 2017. Fluid-driven metamorphism of the continental crust governed by nanoscale fluid flow. *Nat. Geosci.* 10, 685–690. <https://doi.org/10.1038/ngeo3009>.
- Putnis, A., Moore, J., Prent, A.M., Beinlich, A., Austrheim, H., 2021. Preservation of granulite in a partially eclogitized terrane: metastable phenomena or local pressure variations? *Lithos* 400–401, 106413. <https://doi.org/10.1016/j.lithos.2021.106413>.
- Roberts, D., 2003. The Scandinavian Caledonides: event chronology, palaeogeographic settings and likely modern analogues. *Tectonophysics* 365, 283–299. [https://doi.org/10.1016/S0040-1951\(03\)00026-X](https://doi.org/10.1016/S0040-1951(03)00026-X).
- Roberts, D., Gee, D.G., 1985. An introduction to the structure of the Scandinavian Caledonides. In: Gee, D.G., Sturt, B.A. (Eds.), *The Caledonide Orogen - Scandinavia and Related Areas*. John Wiley & Sons Ltd, Chichester, pp. 55–68.
- Rogowitz, A., Huet, B., 2021. Evolution of fluid pathways during eclogitization and their impact on formation and deformation of eclogite: a microstructural and petrological investigation at the type locality (Koralpe, Eastern Alps, Austria). *Tectonophysics* 819, 229079. <https://doi.org/10.1016/j.tecto.2021.229079>.
- Simon, M., Pitra, P., Yamato, P., Poujol, M., 2023. Isothermal compression of an eclogite from the western Gneiss region (Norway). *J. Metamorph. Geol.* 41, 181–203. <https://doi.org/10.1111/jmg.12692>.
- Spieß, R., Groppo, C., Compagnoni, R., 2007. When epitaxy controls garnet growth. *J. Metamorph. Geol.* 25, 439–450. <https://doi.org/10.1111/j.1525-1314.2007.00704.x>.
- Steltenpohl, M., Hames, W., Andresen, A., Markl, G., 2003. New caledonian eclogite province in Norway and potential Laurentian (taconic) and Baltic links. *Geology* 31, 985–988. <https://doi.org/10.1130/G19744.1>.
- Steltenpohl, M.G., Kassos, G., Andresen, A., 2006. Retrograded eclogite-facies pseudotachylytes as deep-crustal paleoseismic faults within continental basement of Lofoten, north Norway. *Geosphere* 2, 61–72. <https://doi.org/10.1130/GES00035.1>.
- Steltenpohl, M.G., Kassos, G., Andresen, A., Rehnström, E.F., Hames, W.E., 2011. Eclogitization and exhumation of caledonian continental basement in Lofoten, north Norway. *Geosphere* 7, 202–218. <https://doi.org/10.1130/GES00573.1>.
- Tamblyn, R., Hand, M., Simpson, A., Gilbert, S., Wade, B., Glorie, S., 2022. In-situ laser ablation Lu–Hf geochronology of garnet across the Western Gneiss Region: campaign-style dating of metamorphism. *J. Geol. Soc.* 179, jgs2021–2094. <https://doi.org/10.1144/jgs2021-094>.



- Treagus, S.H., Treagus, J.E., 1992. Transected folds and transpression: how are they associated? *J. Struct. Geol.* 14, 361–367. [https://doi.org/10.1016/0191-8141\(92\)90092-B](https://doi.org/10.1016/0191-8141(92)90092-B).
- Tveten, E., 1978. Geologisk Kart over Norge, Berggrunnskart Svølvær 1: 250 000. Norges Geologiske Undersøkelse. <https://www.ngu.no/emne/kartinnsyn>.
- Uno, M., Iwamori, H., Toriumi, M., 2015. Transition from dehydration to hydration during exhumation of the Sanbagawa metamorphic belt, Japan, revealed by the continuous P–T path recorded in garnet and amphibole zoning. *Contrib. Mineral. Petrol.* 170, 33. <https://doi.org/10.1007/s00410-015-1185-9>.
- Vrijmoed, J.C., Podladchikov, Y.Y., 2022. Thermolab: a thermodynamics laboratory for non-linear transport processes in open systems. *G-cubed* 23, e2021GC010303. <https://doi.org/10.1029/2021GC010303>.
- Wayte, G.J., Worden, R.H., Rubie, D.C., Droop, G.T.R., 1989. A TEM study of disequilibrium plagioclase breakdown at high pressure: the role of infiltrating fluid. *Contrib. Mineral. Petrol.* 101, 426–437. <https://doi.org/10.1007/bf00372216>.
- Wex, S., Mancktelow, N.S., Hawemann, F., Camacho, A., Pennacchioni, G., 2018. Inverted distribution of ductile deformation in the relatively “dry” middle crust across the Woodroffe Thrust, central Australia. *Solid Earth* 9, 859–878. <https://doi.org/10.5194/se-9-859-2018>.
- Whitney, D.L., Evans, B.W., 2010. Abbreviations for names of rock-forming minerals. *Am. Mineral.* 95, 185–187. <https://doi.org/10.2138/am.2010.3371>.
- Whitney, D.L., Goergen, E.T., Ketcham, R.A., Kunze, K., 2008. Formation of garnet polycrystals during metamorphic crystallization. *J. Metamorph. Geol.* 26, 365–383. <https://doi.org/10.1111/j.1525-1314.2008.00763.x>.
- Zertani, S., John, T., Brachmann, C., Vrijmoed, J.C., Plümper, O., 2022. Reactive fluid flow guided by grain-scale equilibrium reactions during eclogitization of dry crustal rocks. *Contrib. Mineral. Petrol.* 177, 61. <https://doi.org/10.1007/s00410-022-01928-3>.
- Zertani, S., Labrousse, L., John, T., Andersen, T.B., Tilmann, F., 2019. The interplay of eclogitization and deformation during deep Burial of the lower continental crust—a case study from the Bergen arcs (western Norway). *Tectonics* 38, 898–915. <https://doi.org/10.1029/2018tc005297>.